2013

Effect of Surfactant on Dynamics of a Droplet Released in a Quiescent Medium

Abhijit Rao
Louisiana State University and Agricultural and Mechanical College, arao4@tigers.lsu.edu

EFFECT OF SURFACTANT ON DYNAMICS OF A DROPLET RELEASED IN QUIESCENT MEDIUM

A Thesis

Submitted to the Graduate Faculty of the
Louisiana State University and
Agricultural and mechanical College
in partial fulfillment of the
requirements for the degree of
Master of Science

In

Cain Department of Chemical Engineering

by
Abhijit Rao
B.E in Chemical Engineering, Visveswaraiah Technological University,2007
May 2014

This work is dedicated to my parents, friends and family members…

Acknowledgements

I would like to express my sincere gratitude to my advisor Dr. Krishnaswamy Nandakumar for supporting my present study and research, for his patience, motivation and enthusiasm. I cherish the opportunity to be part of enlightening discussions with him on various topics during the course of this work. His guidance has helped me during the course of this research and writing of this thesis. I could not have imagined of having a better mentor for this study. I would also like to thank Dr. Kalliat T Valsaraj for the encouragement, and insightful comments.

My sincere thanks to Dr. Rupesh Reddy who has helped me with my research work in a great way. Special thanks to Dr. Dandina Rao, for allowing me to use the IFT apparatus in his lab. I also thank Dr. Franz Ehrehenseur , who helped me in setting up the experiment and offered wise suggestions which made things lot easier. I would also take this opportunity to acknowledge High Performance Computing (HPC), at LSU, Louisiana Optical Network Initiative(LONI) and XSEDE for providing access to the computational resources. I thank my fellow lab mates in the research group: Tom Scherr, Yuehao Li, Oladapo Ayeni, Guongqiang He, Chenguang Zhang and Aaron Harrington, for the stimulating discussions, which were amazingly fruitful. I appreciate the help provided by Allan Huang in processing the images form experiment. Last but not the least, I would like to thank my parents, family members and friends who have been a source of inspiration and have supported me throughout my life.

This work was made possible by grant received from CMEDS consortium under Gulf of Mexico Research Initiative.

Table of Contents

Nomenclature

A_p : Projected area of droplet in direction normal to its motion [m^2]

C_d : Drag coefficient

C_p : Pressure coefficient

D_n : Diameter of nozzle, [m]

D : Diffusivity [m^2/s]

E : Aspect ratio

F_D : Drag force, [N]

F_s : Interfacial Tension force, [N]

U : Average rise velocity of the droplet, [m/s]

V_d : Volume of droplet at the time of formation [m^3]

V : Corrected volume of droplet after pinch off [m^3]

Greek Alphabet letters

α : Volume of fraction of dispersed phase

γ : Surface curvature

K : Viscosity ratio of dispersed phase to that of continuous phase

ρ_c : Density of continuous phase [kg/m^3]

ρ_d : Density of dispersed phase [kg/m^3]

μ_c : Viscosity of continuous phase [kg/m.s]

μ_d : Viscosity of dispersed phase [kg/m.s]

ψ : Harkins Brown Factor

σ : Surface Tension coefficient [N/m]

Γ : Surface Concentration at the interface [mol/m^2]

Non dimensional Numbers

Re : Reynolds Number

Eo : Eötvos Number

M	:	Morton Number
Ta	:	Tadaka Number
Ci	:	Circulation Number

Abstract

During the 'Deepwater Horizon' accident, dispersants were used as one of the remediation methods to mitigate the ill effects of oil that entered the water column. The dispersants lower the interfacial tension at the oil-water interface and cause the large oil droplets to disintegrate into finer droplets which remain dispersed in the water column for longer times. A dispersant typically is composed of a surfactant and solvent. Surfactants are chemical compounds which are chiefly responsible for the lowering of interfacial tension at oil water interface.

In this study, we have investigated the effect of surfactant on the dynamics of a single crude oil droplet released into the quiescent water column. Experiments have been conducted in a tank with a capacity of about 100 liters, with an oil droplet being released through a nozzle. The droplets ranging from 0.3 to 0.85 cm were produced from three different nozzles. The shape adopted by the emanating droplets varied from spherical to oblate. On addition of the surfactant, sodium dodecyl sulfate (SDS) to water column there occurs reduction in interfacial tension at oil water interface which causes the droplet to flatten. SDS concentrations in water phase were varied in the range from 0 to 750 ppm. The change in the dynamics of the droplet due to the surfactant action has been reported in terms of the departure of the value of rise velocity and aspect ratio from that observed for a rising droplet in absence of surfactant. All experiments were conducted in ambient conditions.

The second aspect of this study presents a numerical model based on finite volume method, which emulates the experimental observations. Volume of fluid method has been used for tracking the oil-water interface. The interfacial tension at the oil-water interface at various concentrations of surfactant is measured by Pendant drop Method using the Axisymmetric Shape Drop technique and has subsequently been used in the simulations. The model developed can be used to predict the behavior of droplets released into the water column during the oil spill.

Chapter 1 Introduction

Droplets represent a fundamental entity in many physical phenomena and industrial processes like liquid – liquid extraction, spraying etc. One of the environmental hazards where role of droplets cannot be ignored is the event of an oil spill. Recently, during the 'Deepwater Horizon' accident in the Gulf Coast in 2010, it has been estimated that about 4.9 million barrels (www.oilspillcommission.gov) of oil was released into the Gulf of Mexico, thus, making it one of the worst ocean spills in recent times. The oil was released into the ocean at the depth of 5000 ft. An ocean column essentially represents a stratified environment, i.e. the density varies (increases) with depth. When the oil is accidentally released into a stagnant environment (ocean water), in huge quantities, the gushing oil loses its momentum energy and results in entrainment of surrounding water and forms a plume. A typical plume is thus a multiphase mixture of oil, gas and ambient water. The plume consists of a gas core, which serves as a source of buoyancy and allows it to rise in the water column. As reported by Socolofsky [1], the presence of cross currents can cause the plume to bend and lead to the fractionation of gas phase from the main plume. The shear interaction between the oil / gas plumes and the ambient fluid results in formation of droplets with wide size distribution[2]. The above process is depicted in the Figure 1.1.

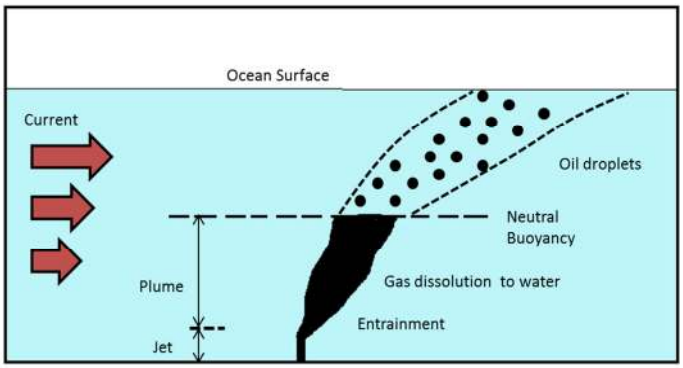

Figure 1.1 Snapshot of ocean water column during oil spill

The oil droplets rising through water column can take following pathways;

a) reach surface if they are large enough, to have significant rise velocities, and coalesce to form surface slicks.

b) The oil on the surface can lose lighter fraction to atmosphere through evaporation and become denser than surrounding fluid and sink.

c) Get trapped (small droplets) in neutrally buoyant regions, not contributing to surface slicks.

d) Get attached to other denser settling particles in water and eventually sink(this phenomenon is known as marine snow).

e) May lose lighter hydrocarbons and eventually reach a density greater than water, and descend to reach ocean floor.

f) The oil on the surface can be carried by surface winds and ocean currents to reach shorelines.

g) Few studies also suggest that wave breaking phenomenon can cause the PAH's (polyaromatic hydrocarbons) in oil on water surface can enter the atmosphere.

h) Many aquatic microorganisms feed on small oil droplets and it may eventually enter the food chain.

Federal Interagency Solutions group consisting of lead researchers from NOAA, USGS and NIST [3] has published a report to estimate the fate of oil that was released during the event. According to it, around 17% of oil was recovered directly by a 'Tophat Recovery system'. The naturally dispersed oil constituted about 13%, which remained suspended in the water column. About 23% of oil was believed to have disappeared through either evaporation or dissolution. Evaporation is restricted to oil slicks, whereas, dissolution is an important mechanism in deep water spills of raw crude containing a larger portion of lighter material. The chemically dispersed amount is estimated to be 16%. The amounts that were burned and skimmed are estimated to be 5% and 3% respectively. The unaccounted oil by any of the above estimates is about 23%, which has been termed as 'other oil' in the report. The fate of this unaccounted oil is yet to be explained.

One of the remediation methods was to spray dispersants to disperse oil in water column. Nearly 2.1 million gallons [4] of dispersant used during 'Deepwater Horizon'. For the very first time, subsea injection was tried and about 30% of total dispersant used towards mitigation, was injected at point of release. Due to lowering of interfacial tension and the existing turbulence the large droplets disintegrate into smaller droplets and disperse in the water column.

The droplets and gas bubbles rising in the column contain plethora of organic components which diffuse into the surrounding water under existing concentration gradients. The presence of these alien components in

water has detrimental effect on marine environment. In order to have an estimate amount of these components entering the water body, it is important to understand the dynamics of droplet, which affects the mass transfer rates. The presence of surfactants further complicates the system. Before getting into a real scale problem, which involves huge swarm of droplets and bubbles, it is important to have a good understanding of fluid dynamics of a single droplet, rising in the water column, in presence and absence of surfactant.

Many studies have been conducted in past for gaining insight on single droplet dynamics. The work of Garner et al. [5], focused on the role of internal circulations on the droplet dynamics. They conducted experiments with a mixture of carbon tetrachloride and cyclohexane as dispersed phase and 83% (by wt.) solution of glycerol in water as a continuous phase. Aluminum particles were added in the dispersed phase to visualize the flow patterns inside the droplet. In their study they also investigated the effect of surfactant addition and concluded that the presence of surfactant retards the internal circulations in the droplet.

The motion of large droplets through immiscible fluid was experimentally investigated by Wairegi et al. [6] for a wide range of Eötvos numbers. They reported different shapes of droplets which included ellipsoidal- and spherical-caps with and without skirts, crescents, biconcave disks, toroids and wobbling irregular droplets.

Winnikow et al [7], studied the motion of droplets in purified systems, and presented results on the behavior of falling organic droplets covering a wide range of Re from 100 to 1000. In their work, they calculated drag force for both non-oscillating and oscillating droplets and identified that at the transition point, a sharp increase was seen in the drag coefficient. In addition they observed that the onset of droplet oscillations was marked with the periodic shedding of vortices behind the droplet. The transient and terminal velocities of the toluene droplets varying from 1 to 7mm in diameter were analyzed by Wegener et.al[8] . They developed a correlation for terminal rise velocities in pure systems. A bifurcation was reported for few droplets, i.e. they exhibited two distinct terminal velocities. Bozzi et al [9], studied steady axisymmetric flow around the droplet at intermediate Reynolds numbers.

The objective of this study is to present results from the experiments conducted on crude oil droplets, released into a quiescent pool of water, containing surfactant. The viscosity ratio, which represents ratio of dispersed to continuous phase, was around 25. The droplets of varying sizes were produced by three sets of nozzles whose internal diameter varied from 1mm to 8.5mm. The dynamics of droplets were observed to change

considerably with increase in the concentration of the surfactant (Sodium dodecyl sulfate) in the continuous phase. The parameters like aspect ratio *E*, which is the ratio of minor to major axis of the droplet; and the rise velocity, were used to report this change. Most of the droplets were found to follow an ellipsoidal regime. However, at higher surfactant concentrations, large droplets exhibited significant wobbling and traced a zigzag path. When the droplet is released initially its surface is devoid of surfactant. But, as it starts rising in the water column, the surfactant gets adsorbed on to the surface of the droplet and brings in changes to the interfacial tension which influences the dynamics of the droplet. The movement of a surfactant molecule from the bulk phase to the interface can be broken into following steps, a) transport of surfactant molecules from bulk phase to region close to oil-water interphase, due to the existing concentration gradient, b) adsorption of surfactant on the surface of an oil droplet. Depending on the local surfactant concentration the interfacial tension reduces and the local shear and turbulence causes the droplet to disintegrate.

A numerical model based on finite volume method, capable of emulating the observations of the experiment, was developed. Volume of fluid was used to perform multiphase simulation, which was able to capture the deforming interface, as the droplet rose in the water column. 2D axisymmetric assumptions were made to perform numerical simulations for droplets which travelled in rectilinear path with no or very insignificant wobbling. A complete 3D simulation was required to demonstrate the dynamics of the large droplets which during its rise in the water column deviated appreciably from the reference axis.

Chapter 2 Droplet Formation

In a liquid –liquid system, droplets are normally generated by forcing a liquid, through an orifice or a nozzle, into a surrounding immiscible liquid which may be rarer or denser than it. Conventionally, the fraction of volume that the liquid being injected to the system occupies is small and it is often referred to as a 'dispersed phase' and the surrounding immiscible liquid is called 'continuous' phase. Depending on the application and need, the nozzle or the opening can be placed either vertical, horizontal or at some angle. The location where the droplet formation takes place depends on the velocity at which the dispersed phase is injected through the nozzle. At a very low flow rates, as the liquid is introduced droplet forms and detaches at the tip of the nozzle. This constitutes the dripping regime. As the flow rate is gradually increased, at a critical flow rate, jet emerges from the nozzle and this velocity at which jet formation takes place is known as jetting velocity denoted by u_{jet}. The droplets are produced from the jet, when the interfacial instability develops on the surface of jet and causes its breakup. The length of the continuous filament extending from the tip of the nozzle to the point where jet disintegrates is known as the 'jet breakup length'. Thermodynamically, the free energy of cylindrical jets do not bear a minimum value, so presence of even a slightest physical perturbation helps in triggering instabilities . Some of these are fast growing and are not damped which ultimately cause jet to breakup. The primary source of this instability that leads to generation of droplets is the presence and action of surface tension. The jet breakup length increases with increase in nozzle velocity until a critical velocity u_{max}. The jet in this regime (between u_{jet} and u_{max}) is laminar and the dynamics of jet remain axisymmetric. The droplets are formed by disintegration of jet and are mono-dispersed in nature. When the nozzle velocity is increased beyond u_{max} the jet loses axisymmetric behavior and breakup length falls. The jet breakup in this regime occurs because of asymmetrical sinuous disturbances. Unlike in laminar regime, the droplets are ejected laterally from the surface of jet and are poly-dispersed. When the flow rate exceeds a critical velocity u_{atm} , a regime known as 'atomization' is observed in which the droplets are again found to be produced at nozzle. During this regime a large number of very fine droplets of non-uniform sizes are formed. Figure 2.1 depicts the variation in jet breakup length with jet injection flow rate. The snapshots from experiment conducted by Masatuni et al[10] depicting these regimes has been shown in Figure2.2 .

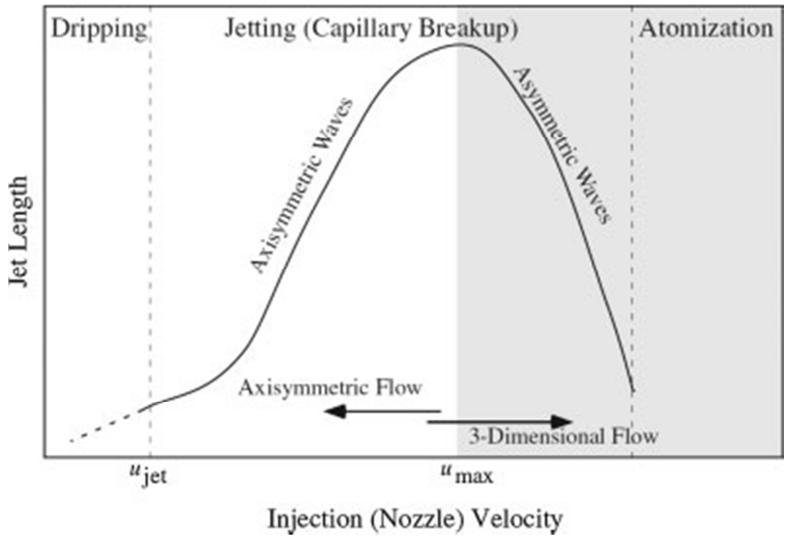

Figure 2.1 Jet breakup Mechanism[11].

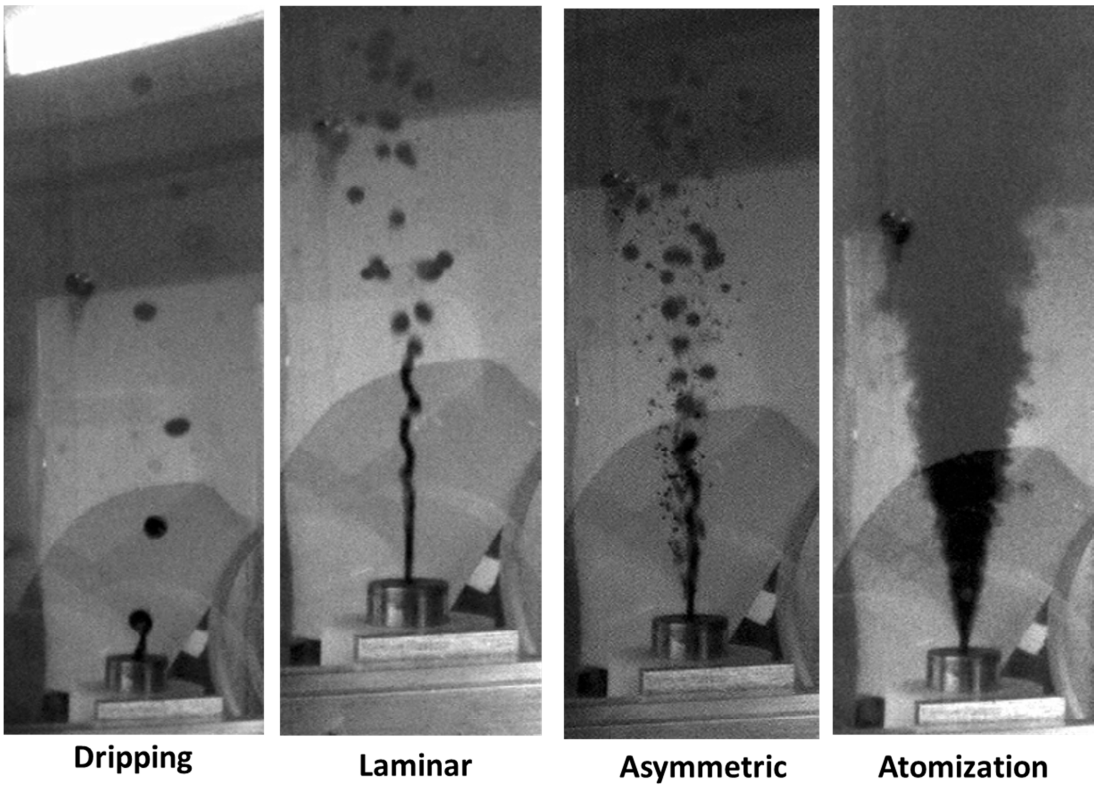

Figure 2.2 Different regimes of jet breakup taken from experiment conducted by Masatuni et. al[10].

2.1 Droplet formation at low rates

In present work we have focused on the dynamics of single droplet moving in the continuous phase and hence the droplet formation during dripping regime will be considered. The drop formation depends on the balance of following forces:

- Buoyancy force
- Interfacial force.

The force due to buoyancy is attributed to the density difference between the dispersed phase and the continuous phase. The buoyancy force tends to separate the droplet from the nozzle whereas the interfacial force acts to keep droplet attached to the nozzle. Under static conditions, there exists opposition between buoyancy and interfacial tension force at the nozzle and the moment the lifting force exceeds the restraining force the droplet pinches off the nozzle.

The size of the droplet pinching off from the nozzle can approximately be calculated through a simple balance between the acting forces. The volume of the droplet V_d clinging to the nozzle is given by,

$$V_d = \frac{\pi D_n \sigma}{g \Delta \rho} \qquad 2.1$$

where D_n is the nozzle diameter, σ is the interfacial tension and $\Delta\rho$ corresponds to the density difference between the dispersed and the continuous phase. The actual volume V_a of the droplet that pinches off is slightly lesser than V_d. During pinch off a small volume of V_d is retained by nozzle. To account for this Harkins [12] proposed a factor ψ which is given by Equation2.2.

$$\psi = {V_a}/{V_d} \qquad 2.2$$

Mori[13] proposed a correlation for evaluation of ψ given by Equation 2.3.

$$\psi = 0.6 + 0.4\left[1 - \frac{D_n}{1.4}\left(\frac{\psi}{V}\right)^{1/3}\right]^{2.2} \qquad \text{valid for } D_n\left(\frac{\psi}{V}\right)^{1/3} < 1.4 \qquad 2.3$$

The pinch off mechanism can be categorized into two stages:

- Lift off
- Necking & Pinch off.

The first stage corresponds to the point when the droplet experiences lift and elongates slightly, once all external forces balance each other. During the second stage the buoyancy force starts exceeding the opposing interfacial force and this exerts a pull and causes necking and finally the droplet gets detached from the main fluid filament when the neck breaks [14],[15]. These stages have been shown in Figure 2.3.

Figure 2.3 Formation of a droplet during experiment and its detachment from the nozzle: lift off stage ; necking and pinch off stage.

2.2 Drop formation at moderate flow rates

At moderate flow rates inertial forces become important. As a result of this a drag force is exerted on the droplet by the continuous phase[16]. The buoyancy and inertial forces tend to destabilize the droplet whereas the drag and interfacial tension forces try to keep the droplet attached to the nozzle. Assuming that fully developed flow is achieved in the nozzle, Meister et al[17] proposed a correlation for calculation of volume of the droplet pinching off, which is given by,

$$V_d = \psi \left[\frac{\pi D_n \sigma}{g\Delta\rho} + \frac{20\mu Q D_n}{D_f^2 g\Delta\rho} - \frac{4\rho_d Q U_n}{3g\Delta\rho} + 4.5 \left(\frac{Q^2 D_n^2 \rho_d \sigma}{(g\Delta\rho)^2} \right)^{1/3} \right] \qquad 2.4$$

where Q refers to the volumetric flow rate, U_n is the average velocity of the dispersed phase, D_f represents the diameter of the detached drop.

2.3 Drop formation during jet break up

As stated earlier the formation of jet occurs when the injection velocity is greater than the jetting velocity. Mister et al [17] developed an expression for critical flow rate which is given by,

$$Q_{jet} = 1.36 \left[\frac{\sigma D_n^3}{\rho_d} \left(1 - \frac{D_n}{1.24\, V_a^{1/3}} \right) \right]^{1/2} \qquad 2.5$$

The estimation of diameter of a droplet resulting from jet break up can be done by using expression proposed by Horvath et.al[18]. The equation is valid in the laminar regime $Q_{jet}<Q \leq Q_{max}$,

$$D_d = D_{j,max}\left[2.06\frac{U_{n,max}}{U_n} - 1.47\ln\left(\frac{U_{n,max}}{U_n}\right)\right] \qquad 2.6$$

where $D_{j,\,max}$ and $U_{n,\,max}$ are the jet diameter and jet velocity at Q_{max}.

2.4 Rate of droplet formation

The rate at which droplet forms often affects processes like heat and mass transfer during the formation stage. The flow patterns developing inside the droplet depends on the rate at which the dispersed phase is introduced through the nozzle [19]. Depending on the rate of injection, the droplet formation can be classified as

- Slow formation
- Fast formation.

During the slow formation of droplet, the dispersed phase is introduced at a very low flow rate, and the droplet is allowed to grow gradually. This eliminates the development of circulations inside the droplet. As a result of this the heat and mass transport occurs purely due to diffusion. However, during fast formation, the momentum of entering fluid causes generation of convection currents inside the droplet phase which enhances mass transfer. Humphrey et al.[19] suggested a parameter called circulation number Ci given by Equation 2.7.

$$Ci = We \cdot Re \qquad 2.7$$

The above equation depicts the transition of flow patterns from circulating to stagnant during the evolution of droplet. Ci has highest value during the initial stages of formation and reaches a minimum value at the time of detachment.

2.5 Formation of satellite drop

Until now we have considered a scenario where pinch off mechanism yields only a single droplet. There are circumstances when multiple droplets of different sizes may generated by the pinch off mechanism. During this regime, the droplets generated can be classified as a primary droplet, which refers to a predominant droplet resulting from a pinch off mechanism and secondary or satellite droplets which are much smaller than the primary droplet. Figure 2.4 shows the stages involved during formation of the satellite droplet. It has been stated that during the evolution of the droplet, neck formation takes place. The buoyancy force exceeds the interfacial forces,

just before the pinch off, the neck elongates and its width decreases, shown in Figures 2.4 (a) to 2.4 (d). Once the droplet disengages, this long filament recoils (Figure 2.4(e)). Satellite drops are generated when the filament is extremely thin, which has been depicted in Figure2.4 (f). The growth of capillary instabilities over the filament causes it to disintegrate into tiny droplets. Thus, satellite droplets can be found in situations where the injection velocity is extremely low. At moderate velocities, once the primary droplet detaches, the incoming dispersed phase from nozzle ensures that the neck remains thick and the satellite droplets thus, are never generated.

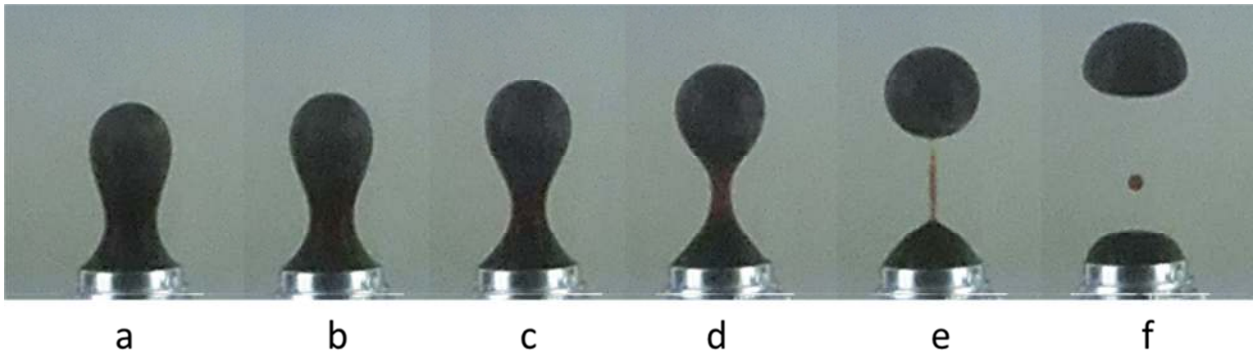

Figure 2.4. Stages which lead to the formation of a satellite droplet.

In the present study, our focus is mainly to analyze the dynamics of moving droplet. A brief discussion on the droplet pinch off mechanism was included to present a complete picture behind the origin of droplets in the system.

Chapter 3 Regimes of Droplet Motion

The behavior of fluid particles in motion in a domain consisting of another fluid differs a lot from that exhibited by rigid particles. The integrity of the surface of a rigid particle is not influenced by the flow of the surrounding medium around it. Further, the purity of the surrounding fluid has a negligible influence on the rigid particle dynamics. However , in case of a droplet , the surface happens to be deformable ,which allows for the shear at the surface, to influence the motion fluid inside the droplet[7]. This gives rise to internal circulations inside the droplet which effectively reduces the drag on the droplet. Hence, the droplet always exhibits (in a pure system free of contaminants) a higher rise velocity than that of a corresponding rigid sphere. In addition to the internal circulation, the flow of the outer fluid around the droplet may bring variation in its shape. In literature[20] the departure of the droplet from spherical is often represented by the term aspect ratio *E*, which refers to the ratio between the minor axis to that of the major axis. Thus,

E=1 Spherical droplet

E<1 Oblate spheroid

E>1 Prolate Spheroid

Thus, the overall drag experienced by the droplet is dependent on the strength of internal circulations and the shape it acquires during its motion.

3.1 Important Dimensionless Numbers and Quantities

This section describes various dimensionless numbers which have been conventionally used by the researchers to classify the regimes for a droplet in motion.

3.1.1 Reynolds Number

The Reynolds number represents the ratio of inertial force to the viscous force. It is given by

$$Re = \frac{d_p v \rho}{\mu} \qquad 3.1$$

where d_p refers to the diameter of the droplet, v is the relative velocity between the droplet and the surrounding medium , ρ is the density of the continuous phase and μ is the viscosity of the continuous phase.

3.1.2 Eotvos Number

Eotvos number measures the relative importance of buoyancy forces to the interfacial tension force.

$$Eo = \frac{g\,\Delta\rho d_p^{\,2}}{\sigma} \qquad 3.2$$

where $\Delta\rho$ represents density difference between the dispersed and continuous phase and σ is the interfacial tension.

3.1.3 Morton Number

It represents ratio of viscous to interfacial forces

$$M = \frac{g\Delta\rho\mu^4}{\rho^2\sigma^3} \qquad 3.3$$

Together with *Eo* it allows to characterize the shape of droplets in the system. Fluids can be arranged in two separate groups, those with high Morton numbers ($M > 10^{-2}$) and those with low Morton numbers ($M < 10^{-6}$). In the present study, the ranges of above dimensionless quantities were: 200<Re<900, 1<Eo<15 and $1\times10^{-10}<M<9\times10^{-8}$.

3.1.4 Viscosity ratio

It is the ratio of viscosity of a dispersed to continuous phase

$$K = \frac{\mu_d}{\mu_c} \qquad 3.4$$

3.2 Freely Moving Droplets

Droplets that rise or fall freely in a continuous medium under influence of gravity are encountered in wide variety of industrial processes. The shape of droplet is result of two competitive forces; the surface tension force, which always tries to restore the spherical shape and the shear force, which tries to deform the droplet. The presence of surfactants lowers the interfacial tension at the interface and allows the interface to stretch more under existing hydrodynamic forces. The viscous droplets generally assume an ellipsoidal shape at moderate Re[20].

3.2.1 Spherical droplets

The spherical droplets exist under scenarios when interfacial tension forces or viscous forces bear more significance over inertial forces. If surface tension are strong , droplets can assume spherical even at moderate

Reynolds Number (Re < 500) [21]. An important thing to note is that under creeping flow conditions i.e. when Re < 1, droplets remain spherical even if the interfacial tensions are exceptionally low.

3.2.2 Ellipsoidal droplets

The moderately sized droplets with equivalent diameters falling in the range 1 to 15 mm often acquire ellipsoidal shape. When *M* is on higher side they normally travel in a steady manner with no oscillating. However, when M is lower they enter a wobbling regime and move with vigorous oscillations.

Figure 3.1 depicts the shape regimes for various droplets studied in the experiment. As shown clearly, droplets at low *M* primarily exhibit ellipsoidal shape. However, an increase in *M* (which indicates a reduction in interfacial tension forces) causes the droplets to enter a wobbling regime.

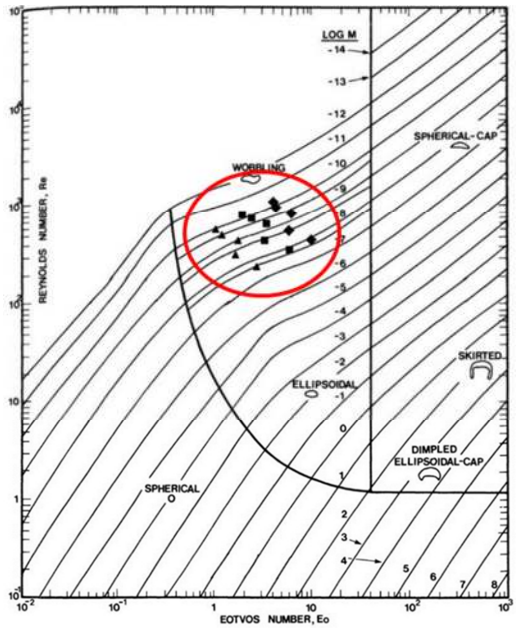

Figure 3.1. Different shape regimes of droplet observed in the experiment(adapted from [20]).

3.3 Parameters used for differentiating regime

3.3.1 Aspect ratio

In most systems where gravitational forces are predominant it is observed that the ellipsoidal droplets acquire oblate shapes. Many correlations have been developed to estimate the aspect ratio for ellipsoidal droplets. For low values of M , Wellek et al. [22] suggested a correlation for E as a function of Eo which is given by

$$E = \frac{1}{1+0.163Eo^{0.757}} \qquad \text{for } E < 40 \text{ , } M \leq 10^{-6} \qquad 3.5$$

Another correlation was developed by Vakrushev and Efremov[23], to estimate the degree of deformation of droplet on basis of its Tadaka Number (*Ta*) which is given by

$$Ta = Re\, M^{0.23} \qquad 3.6$$

In present study, Ta was in the range $2 < Ta < 9$.

$$E = \left[0.81+0.206 \tanh\left\{2\left(0.8- \log_{10} Ta\right)\right\}\right]^3 \qquad 3.7$$

3.3.2 Internal circulations

The internal circulation has a strong dependence on the ratio of viscosities of dispersed fluid to that of continuous fluid and is denoted by K. Higher the ratio, lesser would be the tendency for generation of internal circulations. The purity of the system is another factor which controls the organization of internal flow. Presence of impurities like a surfactant on the surface of droplet impedes the internal circulation and fluid particle starts behaving more like their rigid counterpart. When the flow around is not sufficiently strong, the molecules of surfactant are believed to form a layer which acts a barrier for the transmission of momentum form the continuous phase to the dispersed phase. More details will be discussed in later chapters.

As indicated earlier, the other factor that affects the motion of the droplet is the distortion caused by the external flow to its shape, which essentially, speaks of its departure from its original spherical shape. The system with low interfacial tension has a tendency to induce circulations more easily, but at the same time the droplet also undergoes significant distortion. In case of systems with high interfacial tension the droplets are able maintain their spherical shape, but the internal circulations are not strong enough. Thus, a maximum drag coefficient is encountered by the synergistic effect of internal circulation strength and droplet deformation.

3.3.3 Drag coefficient

The droplet moving in the infinite medium experiences drag force by the surrounding continuous phase. Drag force depends on the velocity of the droplet, the shape of the droplet and also the concentration of surfactant, the presence of which effects the circulations inside the droplet. The hydrodynamic drag force is calculated by,

$$F_D = \frac{1}{2} C_d v^2 A_p \rho \qquad 3.8$$

where C_d is the drag coefficient, A_p is the projected area in the direction normal to the motion of the droplet, U is the relative velocity between the droplet and the continuous phase. Thus, a spherical droplet experiences a lesser drag than an oblate droplet in a system with same degree of contamination because the latter has a higher projected area. In order to evaluate drag force using above relation we need closure for drag coefficient. Many correlations exist in literature which broadly treat C_d to be function of Re, K and Eo.

For creeping flow conditions, Hadamard – Rybczynki solution provides a good approximation for evaluation C_d , which is given by Equation 3.9.

$$C_d = \frac{8}{Re}\left(\frac{2+3K}{1+K}\right) \qquad 3.9$$

The above expression reduces to Stokes law when $K \to \infty$, which represents a rigid sphere. The internal circulation in smaller droplets are very weak, hence, they closely follow Stokes law. For Re < 500 droplets are able retain their spherical shape if interfacial forces are significantly strong. Hamielec et al [24] suggested a correlation :

$$C_d = \frac{3.05\,(7.83K^2+2412K+1080)}{(60+29K)\,(4+3K)\,Re^{0.74}} \qquad 4<Re<100 \qquad 3.10$$

Another correlation valid in this regime is one developed by Rivkind et al.[25] given by equation 3.11.

$$C_d = \frac{1}{1+K}\left[K\left(\frac{24}{Re}+\frac{4}{Re^{1/3}}\right)+\frac{14.9}{Re^{0.78}}\right] \qquad 3.11$$

Feng and Michaelides[26] performed DNS to propose a correlation for C_d applicable for a wide range $5<Re<1000$ and $2< K < \infty$

$$C_d = \frac{4}{(2+K)}\left(17Re^{-2/3}\right) + \frac{K-2}{K+2}\left\{\frac{24}{Re}\left(1+\frac{1}{6}Re^{2/3}\right)\right\} \qquad 3.12$$

The only drawback of this correlation is that it is strictly valid for fluid spheres. However at such high Reynolds number, the fluid droplet undergoes significant deformation and the predicted drag coefficient does not represent a true value. In current case, the droplets appear with significant deformations and hence the existing correlations cannot be used for estimation C_d. A method for estimating C_d using a model built from first principles will be discussed in later sections.

3.3.4 Terminal Rise Velocity

Whenever a droplet is released in the quiescent column, it undergoes acceleration initially under the influence of unbalanced forces. However, after travelling for some distance, the forces around the droplet nullify

each other and the droplet attains a steady velocity, which is often referred to as terminal velocity. An approximate value of terminal velocity can be estimated from the Figure 3.1; knowledge of *Eo* and *M* should be sufficient to fetch corresponding *Re* which can used for determining terminal velocity. For contaminated systems terminal velocity can evaluated using an expression suggested by Clift et al.[20]

$$U = \frac{\mu_c}{\rho d_p} M^{-0.149} \left(J - 0.857\right) \qquad 3.13$$

where $J = 0.94\ H^{0.757}$ $\quad (2 < H \leq 59.3)$ and $J = 3.42H^{0.441}$ $\quad (H > 59.3)$

with $H = \frac{4}{3} Eo\ M^{-0.149} \left(\frac{\mu_c}{\mu_w}\right)^{-0.14}$ $\quad \mu_w$=0.009Pa.s.

Figure 3.2 reveals how the presence of a surface contaminant modifies the internal circulations and hence the rise velocity of air bubbles in water.

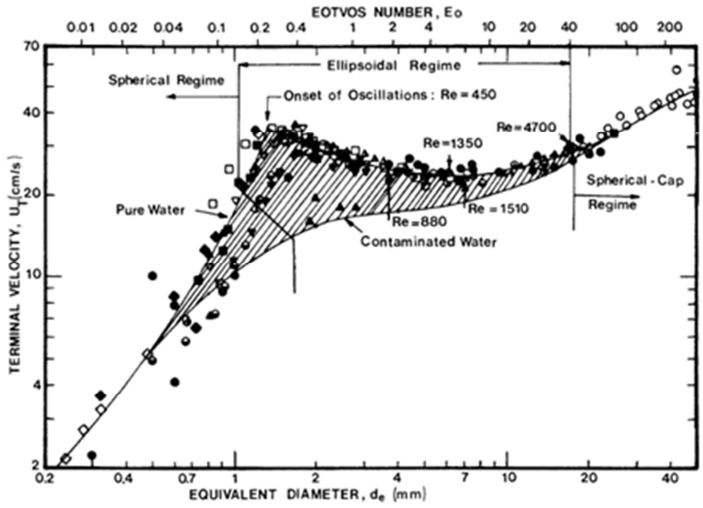

Figure 3.2 Terminal velocity of air bubbles in water for clean and contaminated system (taken from Clift et al[20]).

3.3.5 Wake separation

Before moving to droplets it is important to learn and understand the wake formation occurring behind rigid sphere. Under the creeping flow conditions, the surrounding fluid flowing around the rigid sphere remains attached to the surface and no separation takes place. Wake formation [21] takes place for Re > 20. In steady wake region (20<Re<130) , the wake widens and lengthens with increase in Re and wake bear axisymmetric nature. The

region beyond Re> 130 is marked with the onset of instability and wakes start losing symmetry. Vortex shedding occurs at high Re (400 to 3.5×10^5) wake acquires a 3 dimensional character.

The internal circulations in droplets cause the delay in flow separation. The structure and characteristics of wake behind the droplet plays an important role in determining its trajectory especially when they bear an asymmetric nature. Figure 3.3 shows various categories of wakes that have been reported in literature[7], [27] which are a) steady wake without circulation b) steady wake with circulation and c)unsteady wake with vortex shedding[20],[21]. The axisymmetric wakes are responsible for rectilinear trajectory of the droplet, which is seen for cases with low Re and high *M*. The asymmetric nature of wakes causes droplet to follow a zigzag path and the unsteady wakes are responsible for helical trajectory.

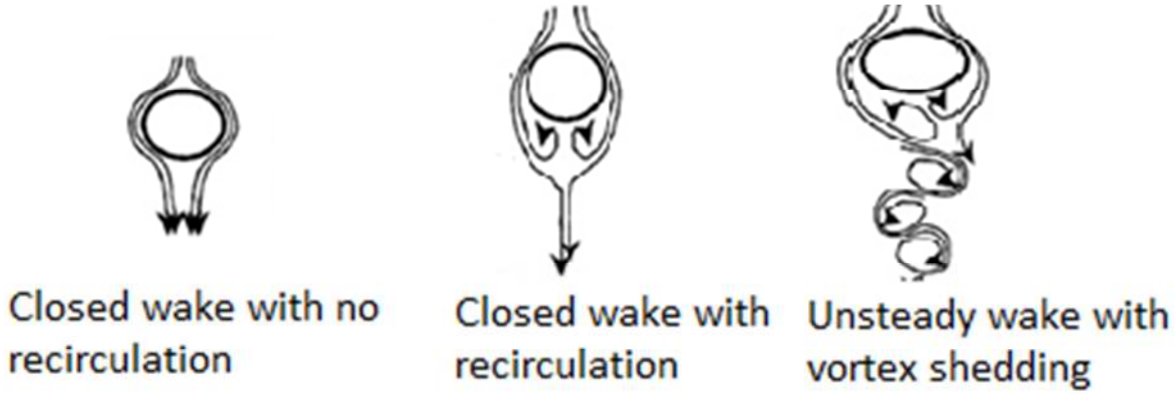

Figure 3.3 Structure of wake behind the droplet.

Figure 3.4 summarizes the various flow transitions observed in the droplets in liquids depending on the droplet size and system purity.

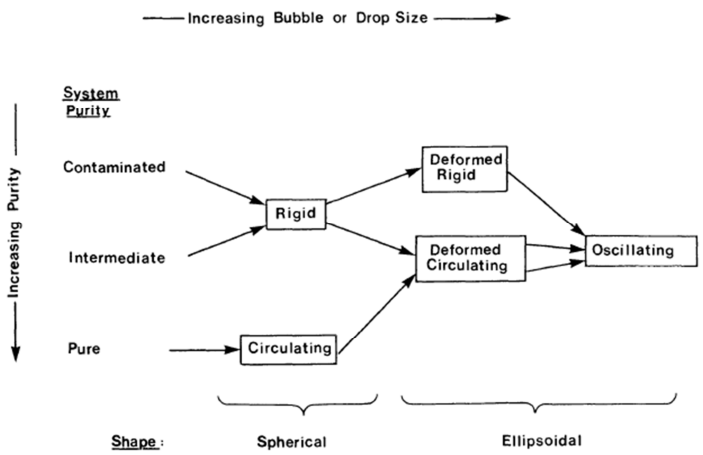

Figure 3.4 Various possible flow regimes of droplet depending on its size and purity of system (from Clift et al[20]).

Chapter 4 Interfacial Tension and its measurement

Interface holds a special significance in determining the dynamics of an immiscible droplet. The characteristic of an interface controls the manner in which the flow organizes itself inside the droplet. To elaborate, a flexible interface is able to transmit the momentum of the outer fluid to the inner fluid more readily when compared to a rigid interface. The change in the behavior of an interface drastically affects the processes like heat and mass transfer occurring around the droplet.

4.1 Origin of surface tension

Surface tension originates because of the non-uniform forces acting on the molecules in the interface. The molecules in the bulk fluid experience equal amount of intermolecular forces, known as cohesive forces, from the surrounding like molecules. However, the molecules at the interface are exposed to two different kinds of forces: forces acting on them due to like molecules (cohesive force) and due to molecules of different species (adhesive force). This has been depicted in Figure 4.1. The molecules at interface are pulled inwards by the intermolecular forces due like molecules surrounding the lower part of molecule. Thus, to attain a lower energy state, the interface acts as stretchable layer. In fluid mechanics, the surface tension is defined in terms of force per unit length.

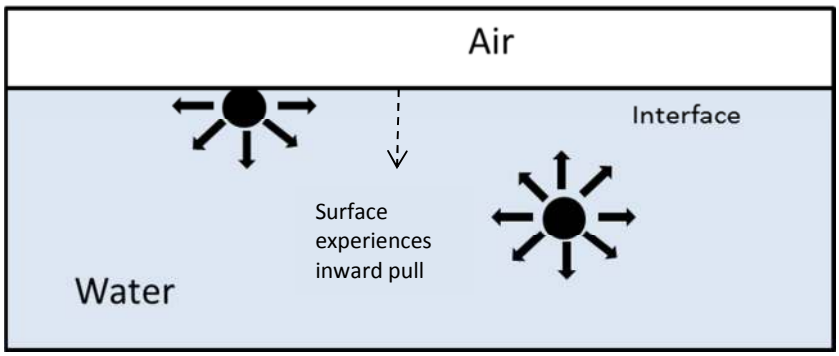

Figure 4.1 Origin of surface tension force.

The surface tension force is given by ,

$$dF = \sigma \, dl \qquad 4.1$$

where σ is the surface tension coefficient and dl is the infinitesimal length across the interface.

4.2 Surfactants

Many applications demand modification of surface tension at the interface. This is often achieved by using additives called surfactants. Surfactants are chemical compounds that modify(normally reduce) the interfacial tension at the interface separating two immiscible phases. A surfactant molecule is composed of two major parts (shown in Figure 4.2),

- Head - hydrophilic end
- Tail - hydrophobic end.

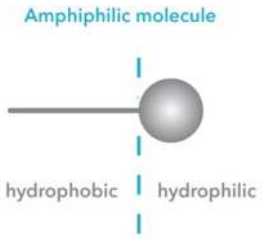

Figure 4.2 Components of a surfactant molecule.

A hydrophobic end is a group which is directed away from water and hydrophilic end is one which has affinity for water. Thus, the adsorption of surfactant onto the interface modifies the surface properties, which reduces the interfacial tension.

4.2.1 Classification

1. Depending on the type of charge on ions that form hydrophobic end , surfactants are classified as
   - Anionic (Sodium dodecyl sulphate, Ammonium lauryl sulphate etc.)
   - Cationic (Benzalkonium chloride, cetyl trimethylammonium bromide etc.)
   - Non-ionic (Glyceryl laurate, Decyl glucoside etc.)
   - Zwitterionic (Lechitin, Cocamidopropyl betaine).
2. Depending on the solubility in the dispersed phase
   - Insoluble (surfactant molecules accumulate at the interface)
   - Soluble (surfactant molecules dissolve in the dispersed phase.

4.2.2 Action of the surfactant

In present study, the surfactant was dissolved in the continuous phase. The transport of the surfactant can be thought to occur in following three stages:

- The transport of surfactant form bulk phase to the region near the interface (called subsurface).
- Adsorption of surfactant on the interface.
- Transport at interface due to the existing convective currents.

The first step basically involves transport due to diffusion and convection (due to the currents in the continuous phase). Once the surfactant molecules are delivered to the subsurface region which is few molecular diameters away from the interface, adsorption comes in to the picture. In most of the cases, the adsorption of the surfactant is presumed to follow Langmuir kinetics. Once adsorbed, surfactant molecules tend to lower the interfacial tension. The relation between the interfacial tension and the bulk concentration of surfactant in the continuous phase is given by Szyszkowski equation

$$\sigma = \sigma_0 - n\, R\, T\Gamma_m \ln(1+K_L C) \qquad 4.2$$

where σ_0 is he interfacial tension in absence of the surfactant , Γ_m is the maximum concentration of the surfactant at the surface, C concentration of the surfactant in the continuous phase , n corresponds to the number of species constituting the surfactant and adsorbing at the interface. For SDS[28], which is univalent ionic surfactant n=2.

The increase in surfactant concentration results in lowering of interfacial tension, but beyond critical concentration of surfactant, interfacial tension attains a constant value. This limit beyond which further addition of surfactant does not bring any change in the surface tension is known as the critical micelle concentration (CMC). This happens because of the fact that the reduction in interfacial tension is solely due to the monolayer of surfactants adsorbed onto the interface. Once monolayer is formed there exists no space on the surface to accommodate additional surfactant molecules and they begin to form micelles. The concept of CMC has been shown in Figure 4.3.

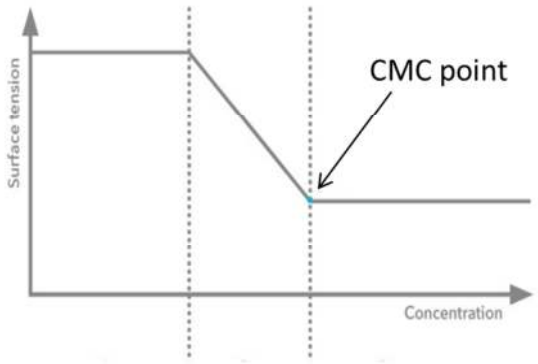

Figure 4.3 Concept of Critical Micelle concentration.

The action of surfactant on the moving droplet is quite complicated. The molecules adsorbing on the surface of a moving droplet are transported to rear end due to the convection existing because of the flow of external fluid around the droplet and as a result, surfactant molecules start accumulating. The non-uniform distribution of surfactant across often is responsible for setting up interfacial tension gradient $\frac{d\sigma}{dc}$, across the surface of the droplet which gives rise to convection currents on the interface. The bulk motion occurs from region of lower IFT to region of higher IFT. This is often referred to as 'Marangoni convection'. Marangoni convection influences the droplet dynamics under circumstances when the inertial forces on the droplet are small. For droplets moving with low *Re*, the surfactant might be able to cover entire surface of the droplet and may form a barrier layer between the dispersed and the continuous phase. Under such a situation, the flow inside the droplet that once existed wanes out and the droplet motion approaches that of a rigid body. This has been depicted in Figure 4.4.

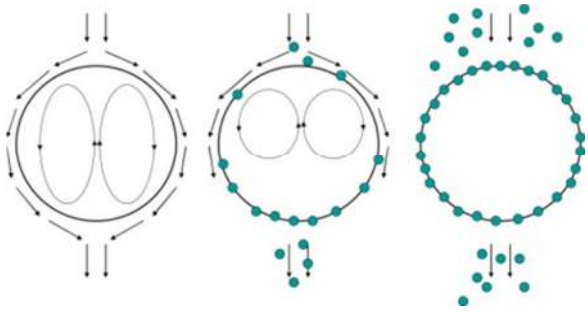

Figure 4.4 Effect of surfactant on the internal circulation of the droplet.

4.3 Measurement of interfacial tension

A variety of methods are available for measuring interfacial tension between two immiscible fluids. Few popular ones are:

- Direct measurement - Using a Microbalance
  - Wilhemy plate Method
  - Du Noüy ring method.
- Measurement of capillary pressure
  - Maximum bubble pressure Method
  - Growing drop Method.
- Gravity distorted drops
  - Pendant drop method
  - Sessile drop method.
- Reinforced distortion of drop
  - Spinning drop method
  - Micropipette method.

In direct measurement technique the interfacial tension is estimated using the force F required to pull the plate (Wilhemy plate Method) or ring (Du Noüy ring method) , off the interface. The following relation is employed for calculation of interfacial tension,

$$\sigma = \frac{F}{p \cos\theta} \qquad 4.3$$

where p is the perimeter of three phase contact line and θ is the contact angle that the liquid meniscus makes with the surface of the object(plate/ ring). The above discussed methods have been depicted in Figure 4.5.

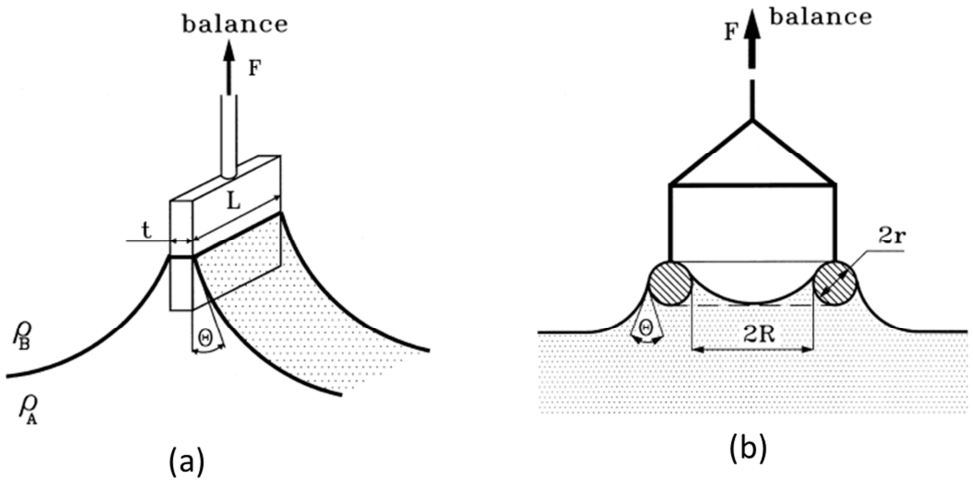

Figure 4.5 Direct IFT measurement techniques a) Wilhelmy plate method b) Du Nouy Ring Method (from Drelich et al[29]).

The tendency of the interface to attain a lower energy state is responsible for the decrease in area witnessed by it. This creates a pressure difference between fluids separated by the interface, with pressure being higher on the concave side. The relation between σ and ΔP, the pressure difference is given by Young-Laplace equation which forms the basis for estimating σ by measuring the capillary pressure,

$$\Delta P = \sigma \left(\frac{1}{R_1} + \frac{1}{R_2}\right) \qquad 4.4$$

where R_1 and R_2 are the radii of curvature.

In "maximum bubble pressure method", a maximum pressure p^*, required to force the droplet out of capillary is measured. p^* is sum of capillary pressure and the hydrostatic pressure. Thus,

$$\Delta P = p^* - \rho g h \qquad 4.5$$

IFT can be estimated using the relation

$$\sigma = \frac{\Delta P\, r}{2}\left(1 - \frac{2r\Delta\rho g}{3\Delta P} - \frac{(r\Delta\rho g)^2}{6\Delta P^2}\right) \qquad 4.6$$

where Δρ is the difference in densities of the two immiscible fluids an r is the radius of the capillary.

IFT can also be measured by shape analysis of the interface. This methodology is particularly more attractive because it demands less instrumentation. The pendant drop and sessile drop techniques fall under this

category. In current work, pendant drop method has been used for measuring IFT at the oil- water interface at different surfactant concentrations. The method will be described in detail in the next section.

Spinning drop Technique is employed for measuring ultralow interfacial tensions. In this method, a drop in a immiscible liquid is filled in a horizontal tube, which is spun about its longitudinal axis. The shape of the droplet depends on the speed of rotation ω. At low velocities, droplet assumes an ellipsoidal shape. However, as the speed is increased it acquires a cylindrical shape. The radius 'r' of cylinder thus formed is dependent on the interfacial tension. Thus , IFT is estimated as suggested by Couper et al[30] , given by

$$\sigma = \frac{1}{4} r^3 \Delta\rho\omega^2 \qquad 4.7$$

4.4 Pendant drop Technique

In this method a pendant drop is formed at the tip of capillary tube. The shape of the droplet formed depends on the competition between the gravitational force and the interfacial tension forces which is best described by the relation suggested by Bashforth and Adams[31]

$$\sigma \left(\frac{\sin \emptyset}{x} + \frac{1}{R_1}\right) = \frac{2\sigma}{b} + \Delta\rho g z \qquad 4.8$$

where R_1 rotates in the plane of paper x is the radius of a point on the interface about vertical axis , $R_2 = \frac{x}{\sin \emptyset}$ rotates in a plane perpendicular to paper and about axis of symmetry, $\emptyset$ is the angle that R_2 vector makes with the axis of symmetry and b is the radius curvature at apex of curvature. Many techniques are available for evaluation of σ through drop shape.

A simple form of shape evaluation has been depicted in Figure 4.6, in which parameters 'd' and 'D' are to be evaluated from the experimentally derived images. The interfacial tension is calculated as [32, 33],

$$\sigma = \frac{\Delta\rho \, g \, D^2}{H} \qquad 4.9$$

where D is the equatorial radius and d is the radius at a distance D from the top of the droplet. H is a parameter which often depends on the shape factor S given by Equation 4.10.

$$S = \frac{d}{D} \qquad 4.10$$

Stauffer et al[33] have provided 1/H v/s S plot for various range of S. In this study, we make use of axisymmetric drop shape analysis technique for estimating, described in the next section.

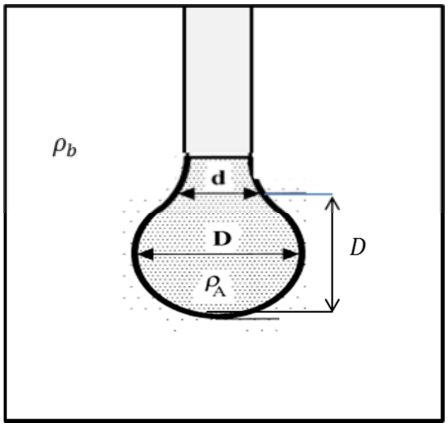

Figure 4.6 Pendant drop technique.

Axisymmetric Drop Shape Analysis (ADSA)

The IFT can be evaluated by image analysis software which matches the profile of pendant drop with one predicted from Brashfort-Adams equation. One such method known as ADSA technique was proposed by Rotenberg et al[34] , in which a scheme was developed to determine the liquid-liquid interfacial tension from the shape of axisymmetric meniscus. An objective function representing error between the observed profile and the one obtained by solving Laplace equation of capillarity was minimized numerically to obtain σ.

Since we are considering an axisymmetric droplet, the profile can be represented by x-z coordinate system. Further, x and z can be expressed in a parameterized form as x = x(s) and z = z(s) with s being the arc length measured from point 'o' in Figure 4.7. Referring to the geometry in Figure 4.7, we arrive with,

$$\frac{dx}{ds} = \cos \emptyset \qquad 4.11$$

$$\frac{dz}{ds} = \sin \emptyset \qquad 4.12$$

Further the rate of change in Ø is given by,

$$\frac{1}{R_1} = \frac{d\emptyset}{ds} \qquad 4.13$$

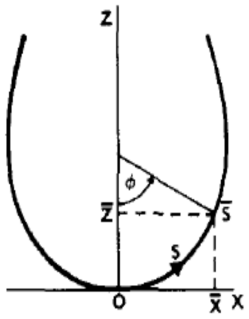

Figure 4.7 IFT measurement using ADSA technique from Profile of a pendant drop (Rotenberg et al [34]).

Combining equations 4.8 and 4.13 we get,

$$\frac{d\emptyset}{ds} = \frac{2}{b} + \frac{\Delta\rho g z}{\sigma} - \frac{\sin\emptyset}{x} \qquad 4.14$$

The profile of the droplet can be obtained by integrating the above differential equations with boundary conditions $x(0) = z(0) = \emptyset(0) = 0$.The experimental measured curve and the profile obtained by solving equations are utilized to define an objective function which describes the error between the two profiles. If profile form experiment is defined by u_n, which represents points on interface and if $v = v(s)$ is the profile from calculated Laplacian solution then objective function can be expressed as [34],

$$E = \frac{1}{2}\sum_{n=1}^{N} [d(u_n, v)]^2 \qquad 4.15$$

where (u_n, v) is the normal distance between the curves $u_n$and v. The error E is minimized through appropriate optimization procedure and correct value of σ is obtained.

4.5 Dynamic and Equilibrium IFT

In a system containing a surfactant either in continuous or dispersed phases, transport of surfactant from bulk portion of phase containing it to the interface occurs entirely by the process of diffusion. During the formation of pendant droplet the dispersed phase is injected into quiescent medium at a very slow rate and hence the convective currents are fairly weak. Once a droplet is formed at tip of the capillary nozzle, IFT measurements are made. When the interface is free from the surfactant the interfacial tension has value corresponding that of pure system often represented by σ_0 . However, with transportation of surfactant molecules to the interface, the properties of interface changes and the interfacial tension drops. The lowering of interfacial tension depends on

the surface concentration of the surfactant and is given by Szyszkowski equation described earlier in the chapter. Thus, as more and more surfactant molecules get adsorbed on to the interface, a further fall in values of interfacial tension is observed. This time dependent variation in values of IFT is termed as 'dynamic IFT'. Figure 4.8 shows a typical dynamic IFT curve from Chen et al. [28], for carbon etrachloride –water system for three different surfactants triton, SDS and DTMAC. After long time of exposure of droplet to surfactant environment, equilibrium is attained and IFT approaches a steady value which is termed at Equilibrium IFT. Figure 4.9 depicts the Equilibrium IFT curve against different surfactant concentrations for carbon tetrachloride –water system. Beyond CMC the increase in surfactant concentration does not help in lowering of IFT.As equilibrium IFT can be attained only after a long time, a method proposed by Hunsel et al. [35] is normally used to estimate the equilibrium IFT value from the dynamic IFT data. The method is based on the fact that the main mechanism guiding the transport of surfactant is diffusion. The suggested method involves plotting dynamic IFT against $t^{-1/2}$ and extrapolating the curve to $t = \infty$, shown in Figure 4.10.

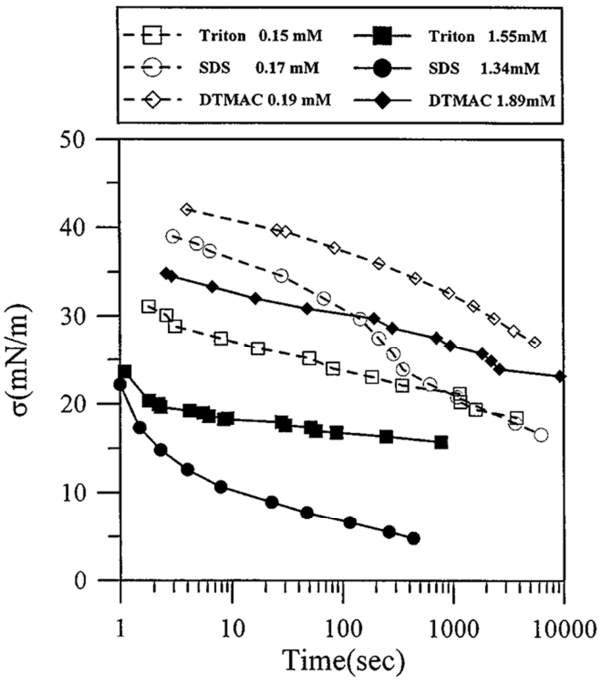

Figure 4.8 Dynamic IFT for CCl_4- water system for various surfactants at different concentrations [28].

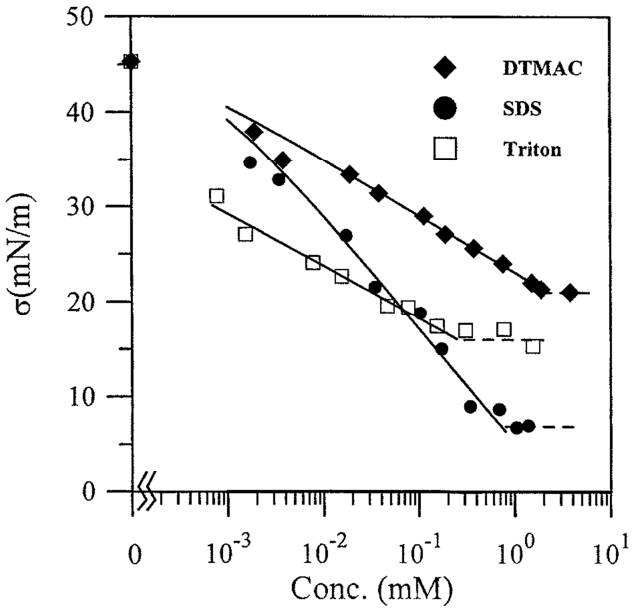

Figure 4.9 Equilibrium IFT for CCl_4 water system for various surfactants [28].

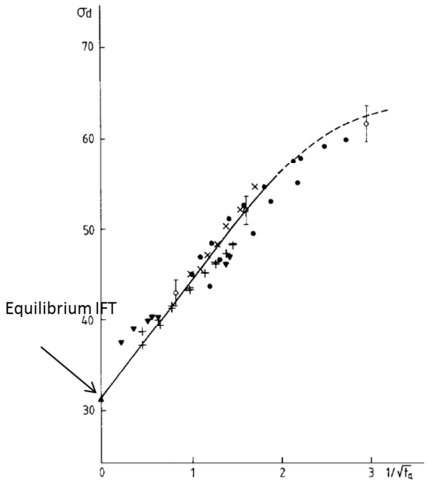

Figure 4.10 Determination of equilibrium IFT from dynamic IFT [35].

Chapter 5 Experiments

A brief discussion on the experimental setup and procedure will be covered in this chapter. The first section deals with the experiments related to single crude oil droplets released in the quiescent water column containing surfactant. The later part of the material describes experiments on IFT measurement using Pendant drop technique.

5.1 Single droplet experiments

The experimental setup consists of a vertical rectangular column made of acrylic glass (PMMA), with height of 100 cm and square base of length 30 cm, which is filled with tap water. The assembly of all major components is shown in Figure 5.1. The dispersed phase, crude oil, is released into the stagnant pool of water through nozzle with the help of a syringe pump. A long PTFE tube is used to connect the syringe mounted on syringe pump and the nozzle. The crude oil used in the experiments was taken from Bosco Field, LA. In this study, an anionic, soluble surfactant, Sodium dodecyl sulfate (SDS 95 %) supplied by Sigma Aldrich Inc. has been used. The properties of these materials can be found in Table 5.1. The crude oil is injected in a controlled manner such that only a single droplet is released at a time. Three nozzles of internal diameters ranging from 1mm to 8.5mm are used to produce crude oil droplets with varying diameters. The tip of all nozzles that were used was well machined. The specifications of nozzles used have been illustrated in Table 5.2. Since the dimension of the tank is far greater than the droplet size, the effect of the walls on the dynamics of droplets is minimal.

The images of droplets are captured using a high speed camera, Canon® EX-ZR200, capable of capturing multiple images at the shutter speed of 1/1000 second. The system is illuminated using 60W fluorescent lamps kept at the corners of the tank. A background sheet is placed to improve the quality of images. The processing of images is done by subtracting the background and converting it into binary image by using a threshold feature available in ImageJ®.The densities of the continuous and dispersed phases are measured using DMA HP density meter and the Ostwald viscometers are used for measuring their viscosities.

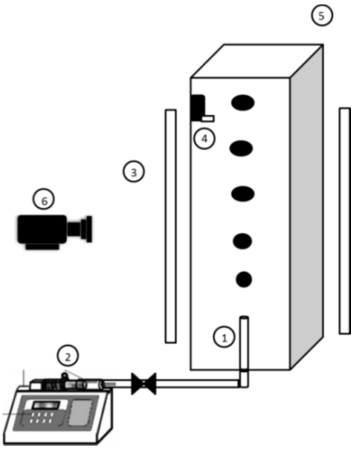

Figure 5.1 Schematic representation of experimental setup 1) nozzle 2) syringe pump 3) Illuminating system 4) submersible pump 5) water column 6) camera.

Table 5.1 Physical properties of the materials/reagents used in the experiment.

Physical properties @ 25 deg C	
Dispersed Phase : Crude Oil	
Origin	Bosco Field,LA
Density	888.8 kg/m^3
Viscosity	25.25 cP
Continuous Phase : Water(tap)	
Density	998 kg/m^3
Viscosity	1cP
Surfactant : Sodium dodecyl sulfate (SDS) - MW 288.372 g/mol	

Table 5.2 Specifications of the nozzles.

	A1	A2	A3
ID(mm)	1.0	2.65	8.5
Droplet dia(mm)	3.1-4.7	4.4-6.1	5.5-8.5
Material	Glass	Glass	Steel

Experiments were conducted at different concentrations (viz. 0, 100, 250,500 and 750ppm, shown in Table 5.3) of surfactant SDS, in the continuous phase. For each concentration of surfactant, around 20 runs of the

experiment were performed. The tank was scrupulously cleaned after each experiment and the water was replaced before surfactant concentration in the continuous phase was graduated to a higher level. After the surfactant addition, the water in tank was kept under circulation with the help of a small submersible pump, for an hour. This was done to ensure a sufficient mixing. The water in the column was later allowed to reach a quiescent state, before oil droplets were introduced into the system. The mass of oil that accumulated on the surface was removed intermittently. All experiments were conducted at ambient conditions.

Table 5.3 Range of surfactant concentration used in the experiment.

Experiment #	SDS concentration	
	(ppm)	(mol/lit)
1	0	0
2	100	3.46×10^{-4}
3	250	8.67×10^{-4}
4	500	17.34×10^{-4}
5	750	26.01×10^{-4}

The diameter of the oil droplet was estimated from the sequence of images taken near the tip of the nozzle, at the time when the droplet was about to pinch off from the nozzle ('A' in Figure 5.2). The measurements were done on 20 droplets and average value was calculated. The rise velocity was obtained by processing high definition video taken from the camera. The average rise velocity was estimated by noting (the time required for 15 droplets to travelling a distance of around 70cm (pt 'B' to 'D' in Figure 5.2); the referenced origin being located about 10 cm above the release point. The residence time of the droplets in the tank varied between 10-15 s. The shape change in droplet was expressed in terms of an aspect ratio 'E', which essentially gave extent of its departure from spherical shape. For aspect ratio measurement, the images were captured near the upper section of the tank, between 'C' and 'D' in Figure 5.2.

$$E = \frac{Minor\ Axis}{Major\ Axis}$$

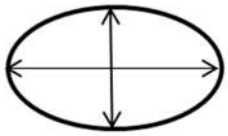

$$Average\ rise\ velocity = \frac{z_{BD}}{\Delta t}$$

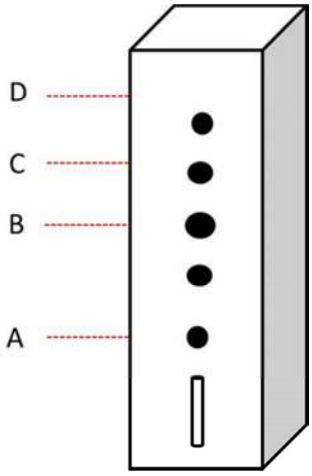

Figure 5.2 Parameters used in the experiment for analyzing droplet dynamics.

5.2 Interfacial tension Measurement in Ambient Cell

The interfacial tension (IFT) at the oil-water interface is lowered on addition of surfactant. To measure this variation in IFT at different surfactant concentrations, pendant drop method was used. IFT was evaluated using Axisymmetric Drop Shape Analysis Technique(ADSA) [34]. The experimental setup shown in Figure 5.3 consists of an optical cell, which has a capillary tube, made of haste alloy, fitted to its lower face through which oil is injected. The diameter of the capillary tube is 1.4mm.The images were captured by a high quality digital camera, capable of recording images at a high frame rate. The video recorder was connected to computer installed with Image processing software. A simplified schematic representation is shown in Figure 5.4.

The continuous phase (water) containing surfactant is drawn into the optical cell through gravity. Once the cell is filled, oil is injected slowly by a syringe, to form an axisymmetric pendant drop at the tip of the capillary tube. The images of the pendant droplet are used to obtain the interface profiles. The interfacial tension is computed by fitting a curve respecting Laplace equation of capillarity, to the shape and profile of the pendant drop. The curve fitting exercise was done by the image analysis software. A description on methodology has already been given Chapter 4; more details can be found in Rio et al [36]. To obtain high quality results, the pendant drop technique requires extreme cleanliness. Hence, before each experiment, entire system is thoroughly cleaned with toluene, acetone and distilled water and dried with a stream of dry air, to ensure a contaminant free system. All IFT measurements in the present study are done at 298K.

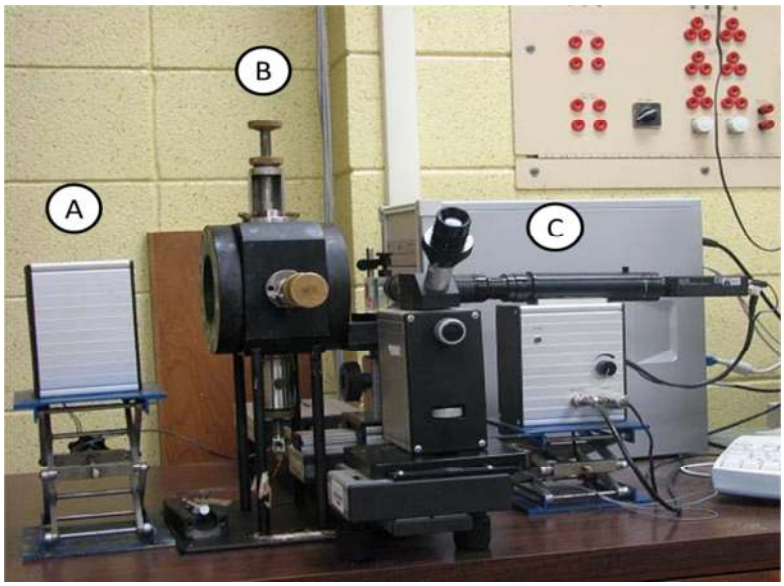

Figure 5.3 Picture of Ambient cell for measuring IFT A) Illuminator, B) Optical Cell and C) Video recorder.

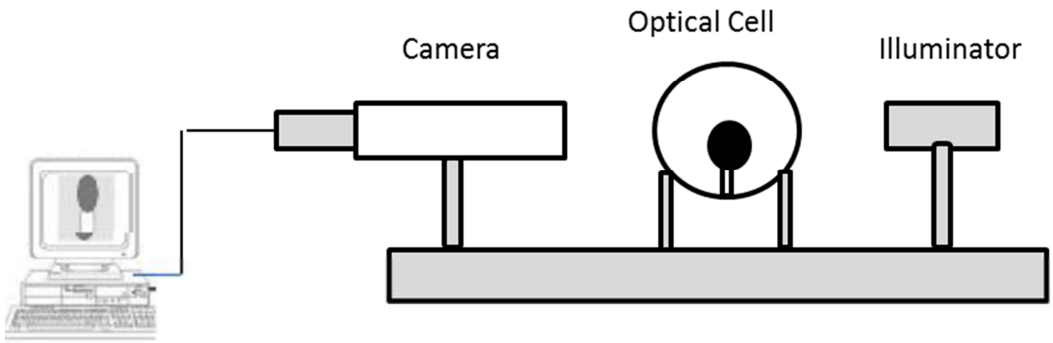

Figure 5.4 Experimental Setup for IFT measurement.

Observations

As soon as a stable pendant droplet is formed, the gradient in concentration of surfactant enables its transport from continuous phase to region near the oil-water interface. Then, the surfactant molecules get adsorbed on to the surface of the droplet. The adsorption of surfactant molecules leads to the increase in its surface concentration at the interface and results in lowering of the interfacial tension. The plot for dynamic IFT for oil-water interface at 100 ppm concentration SDS in continuous phase is shown in Figure 5.5. Figure 5.6 shows the

static pendant drops formed at the tip of capillary nozzle at different surfactant concentrations. If the IFT values are measured for a long time, steady equilibrium value is reached.

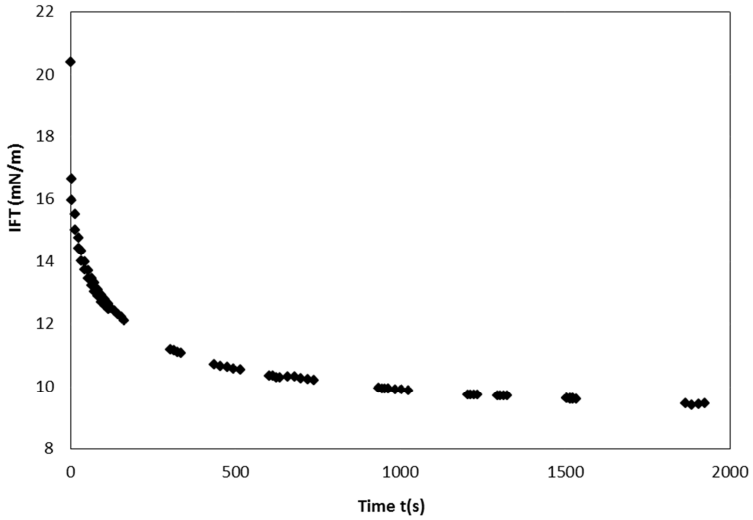

Figure 5.5 Dynamic IFT for SDS concentration of 100ppm.

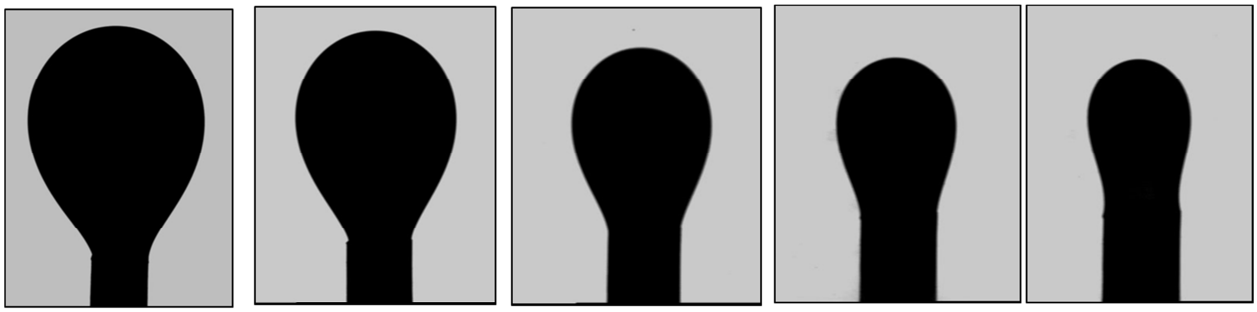

Figure 5.6 Static axisymmetric pendant droplets at various surfactant concentrations.

As explained in Chapter 4, equilibrium values of IFT were extracted from dynamic IFT data by plotting dynamic IFT against $t^{-1/2}$ and extrapolating the curve to $t = \infty$. Figure 5.7 demonstrates the procedure followed in obtaining equilibrium IFT values.

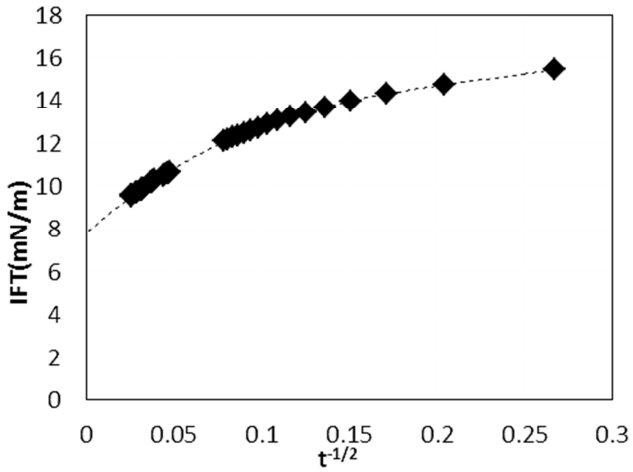

Figure 5.7 Extraction of Equilibrium IFT from dynamic IFT data as suggested in Hunsel et al[35].

Figure 5.8 shows a plot of Equilibrium IFT v/s the surfactant concentration. Clearly, the IFT reduces with increase in concentration of surfactant SDS. However, as it was mentioned earlier, there exists a value, beyond which a further increase in concentration doesn't change the IFT. Such a concentration is called critical micelle concentration (CMC, not shown in Figure 5.8). The actual lowering of IFT is attributed the monolayer formed by the adsorbed surfactant at the interface. Thus, beyond CMC, the presence of monolayer ensures that there exists no space on the interface for adsorption and the surfactant molecules start forming micelles. In present study, the concentration of surfactant in the continuous phase was well over the CMC limit.

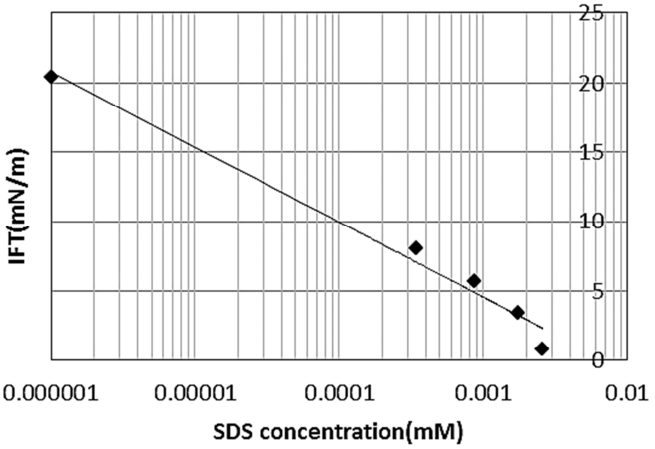

Figure 5.8 Equilibrium IFT as function of SDS concentration.

Curve fitting of the above obtained experimental data with Szyszkowski equation given by Equation 4.2 yields Γ_m , maximum surface concentration and K_L , Langmuir adsorption constant; the values were found to be 6.45×10^{-7} mol/m^2 and 78.8 m^3/mol respectively.

The transport of surfactant from the bulk phase in case of a static droplet is purely by diffusion which is followed by its adsorption. The molecules experience two resistances – one due to diffusion and another due to adsorption-desorption process. Since diffusion is a slow process (for a stagnant system diffusion length is infinite[37]), the time taken for attaining equilibrium surface concentration is fairly long. However, when the droplets are in motion, the convective flux is more dominant than the diffusive flux at the front edge of droplet. This helps in a quick and an efficient delivery of surfactant molecules to the sub-surface (region near the interface with few molecular thickness) from the bulk fluid and hence the time taken to reach an equilibrium adsorption state should be much lesser. The diffusion length in this case falls abruptly and can considered comparable to that of adsorption length. Thus, the time taken to reach equilibrium state depends on the adsorption timescale(described in Chang et al. [37]). The adsorption length is given by

$$l = {\Gamma_m}/{C_0} \qquad 5.1$$

where C_0 is the concentration in the continuous phase. The adsorption timescale depends on the dimensionless length ${l}/{\Gamma_m K_L}$.The time required for the surface concentration to attain 95% of equilibrium concentration is given by,

$$t_{95} = C_{95}\left[\frac{l(\Gamma_m K_L)}{D}\right] \qquad \text{for } {l}/{\Gamma_m K_L} \ll 1 \qquad 5.2$$

$$t_{95} = C_{95}\left[\frac{(\Gamma_m K_L)^2}{D}\right] \qquad \text{for } {l}/{\Gamma_m K_L} \gg 1 \qquad 5.3$$

where C_{95} is a constant given by $C_{95} = {1}/{C_0 K_L}$ as suggested in Franses et al[38] and D is the diffusivity of the surfactant in bulk phase. Table 5.4 shows the details regarding the adsorption length and timescales required to reach an equilibrium state.

Table 5.4 Time required for surface concentration to reach 95% of equilibrium surface concentration.

C_0 (ppm)	C_0 (mol/m3)	$K_L C_0$	C_{95}	l (m)	t_{95} (s)
100	0.3467	27.34	0.0365	1.86×10^{-6}	4.4×10^{-3}
250	0.8669	68.35	0.0146	7.44×10^{-7}	7.1×10^{-4}
500	1.7338	136.71	0.0073	3.72×10^{-7}	1.8×10^{-4}
750	2.6008	205.06	0.0048	2.48×10^{-7}	7.8×10^{-5}

Chapter 6 Numerical Methodology

Apart from experimental work, a numerical analysis was also carried out to emulate the droplet dynamics observed in the experiment. It was seen during the experiment that the smaller droplets exhibited axisymmetric behavior even at higher concentrations of surfactant in the continuous phase. Hence, 2D axisymmetric simulations were performed to save on computation effort needed to solve the governing equations. Larger droplets deviated significantly deviated from the central axis and hence demanded full 3D simulations. All simulations were carried out on supercomputing facility available at High Performance Computing, LSU.

The system consist of two distinct phases; droplet forms the dispersed phase and the water represents the continuous phase. The fluid properties differ a lot, between these phases and this should be captured by the numerical domain efficiently. Further, the success of a numerical model depends how accurately and efficiently is the interface is tracked, especially in a system where the deformations change the shape of the interface significantly. Numerical methods employed for tracking moving interface have been briefly explained in the next section.

6.1 Evolution of Interface tracking Methods

Many methods have been proposed in the literature for tracking the interface. Interface localization methods are broadly classified as :

- Interface Tracking Method
- Interface Capturing Method.

In interface tracking, the interface is represented by set of computational points called nodes. The movement of the interface is achieved by the adjusting the position of the nodes on the interface. Interface tracking approaches are known to provide great accuracy, but they are not employed in situations where interface motion is severe.

In interface capturing approach, an artificial scalar field is employed for the description of the interface. The schemes based on this approach are inherently able to efficiently handle topological changes brought into interface. However, the flexible interface description often poses challenges concerned to mass conservation and the treatment of discontinuities across the interface.

6.1.1 Interface Tracking Methods

6.1.1.1 Volume Tracking

The marker and cell method for interface tracking was introduced by Harlow et al[39] which was implemented on a fixed mesh. The method has been extended in volume tracking method in which a marker quantity is used to reconstruct an interface within the computational cells. The marker entities are located in the region near interface and are advected in the domain in a Lagrangian manner.

6.1.1.2 Immersed Boundary method

This method was suggested by Peskin et al[40], in which mathematical formulation consisted of both Eulerian and Lagrangian variables. The eulerian variables are defined on a fixed mesh whereas Lagrangian variables are associated with a curvilinear mesh which moves freely through the domain.

6.1.2 Interface Capturing Method

In these methods the interface is built by appropriate scalar variables such as volume fraction function.

6.1.2.1 Level Set method

Level set method was first proposed Osher et al[41] ,in which the interface is represented by a certain contour of a smooth function. In this method, a signed distance function is used , which essentially means that, in each point, the level set function is the closest distance to the interface, with positive or negative sign depending on in which fluid the point is. It relies on the introduction of a function $\emptyset$ whose zero level-set represents the interface i.e $C(t) = \{(x, y)|\emptyset(t, x, y) = 0\}$. The interface is advected by the equation,

$$\frac{\partial \emptyset}{\partial t} + u \cdot \nabla \emptyset = 0 \qquad 6.1$$

And normal and curvature of the interface are expressed as ,

$$n = {\nabla \emptyset}/{|\nabla \emptyset|} \quad \text{and} \quad K = \nabla \cdot n \qquad 6.2$$

The main drawback of the originally proposed level set method is that mass is not conserved. In a conventional level set method, $\emptyset$ can experience a shocks which may make its computation highly inaccurate, and hence it is not preferred in situations where the interface varies drastically. To avoid this, a procedure is carried out, where the function $\emptyset$ is initialized as a signed distance function prior to the evolution and then subsequently reinitialized to

be a signed distance function after regular periods during the evolution. The re-initialization procedure is all about solving the following equation,

$$\frac{\partial \emptyset}{\partial t} = \text{sign}(\emptyset_0)\ (1-|\nabla \emptyset|) \qquad 6.3$$

where $\emptyset_0$ is the function to be reinitialized and $\emptyset$ is the sign function.

6.1.2.2 Volume of Fluid Method

Volume of fluid VOF method was proposed by Hirt et al. [42]. This formulation has been developed for two or more fluids which are non-interpenetrating. A phase is represented by volume of fraction α. A value of α=1 represents a dispersed phase whereas $\alpha = 0$ represents a continuous phase. Interface is a represented by a diffused region where α takes values between 0 and 1. The method is naturally conservative, has a fast convergence and a reasonable accuracy [43]. The VOF method works on a fixed grid and the position of interface is determined by the solution of a scalar balance equation for the volume fraction α (which is ratio of volume part filled with dispersed phase to that of total control volume) given by,

$$\frac{\partial \alpha}{\partial t} + \nabla \cdot (\mathbf{v}\alpha) = 0 \qquad 6.4$$

Since α happens to be a discontinuous function; standard upwind finite-difference schemes diffuses the interface, which is highly undesirable. It is normal to adopt a staggered grid representation for velocity vectors, i.e. u , v and w are discretized at the yz , xz and xy face centres respectively, whereas all scalar quantities are calculated at cell centres. The main demerit of this method is due to the discontinuity in VOF method, the normal and curvature that are computed from α are not very accurate[44]. In VOF method, the interface is reconstructed from α field.

6.1.3 Geometric reconstruction scheme

Geometric reconstruction scheme represents the interface in a piecewise linear manner which is shown in Figure 6.1. This method known as PLIC (Piecewise linear interface calculation) was developed by Young et al. [45]. It is based on the assumption that the interface in each cell has a linear slope and this shape of the interface is used for calculation of advection of fluid through the cells in the computational domain (Figure 6.1). The first step in this scheme involves calculating the position of the linear interface relative to the center of each partially- filled cell (cell containing both dispersed as well as continuous phases), based on the information about the volume fraction and its derivatives in the cell. In the second step is the amount of fluid advecting through each face is

evaluated using the computed linear interface representation and information about the normal and tangential velocity distribution on the face. The last step involves calculation of volume fraction in each cell by utilizing balance of fluxes evaluated in the earlier step.

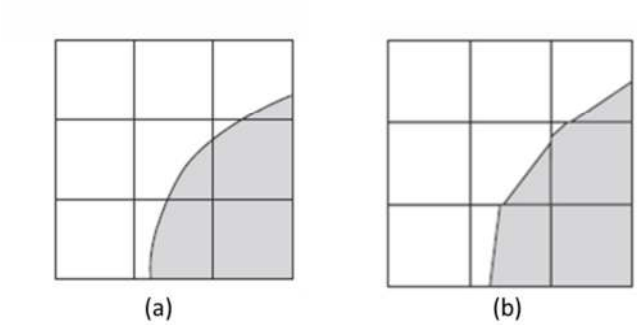

Figure 6.1 a) Actual Interface, b) Interface represented by geometric reconstruction (piecewise linear) scheme.

Having explored numerical methods that are available for simulating multiphase systems, the mathematical model used in current study will be described in the next section.

6.2 Mathematical Model

In this section, the capabilities of Computational Fluid Dynamics in emulating experimental observations have been explored. A numerical model based on finite volume method is developed using a commercially available code, ANSYS Fluent®. It has been mentioned earlier that the smaller droplets exhibited axisymmetric behavior and hence 2D axisymmetric simulations can be done to mimic their behavior. However, this is not true for larger droplets, which require 3D simulations.

The numerical model has been formulated with following assumptions;

1) The fluids involved are immiscible, viscous, incompressible and Newtonian.
2) The flow is isothermal.
3) The interfacial tension across the interface was assumed to bear a constant value.

6.2.1 Governing Equations

We make use of Volume of Fluid scheme, which has been described earlier in the chapter. A single momentum equation (Equation 6.6) along with the continuity equation (Equation 6.5) is solved in the entire domain and the calculated velocity field is shared between the phases.

$$\partial\rho/\partial t + \nabla\cdot(\rho\mathbf{v})=0 \quad (6.5)$$

$$\partial(\rho\mathbf{v})/\partial t + \nabla\cdot(\rho\mathbf{v}\mathbf{v}) = -\nabla p + \nabla\cdot[\mu(\nabla\mathbf{v}+\nabla\mathbf{v}^{T}]+\rho\mathbf{g}+\mathbf{F_s} \quad (6.6)$$

where ρ and μ are the volume fraction averaged properties given by,

$\rho = \sum \alpha_q \rho_q$; $\mu = \sum \alpha_q \mu_q$ where α_q is the volume fraction of phase 'q'.

In equation 6.6, **F** accounts for the body forces; in current case it refers to force due to interfacial tension, which is calculated according continuum surface force (CSF) model[46] given by,

$$F_s = \sigma \, \rho\gamma \nabla\alpha / \langle\rho\rangle \quad (6.7)$$

where ρ is volume averaged density, $\sigma$is surface tension coefficient, γ is local surface curvature given by,

$$\gamma = \nabla\cdot\hat{n} \quad (6.8)$$

with $\hat{n}$ being unit surface normal vector given by $\hat{n} = \frac{\nabla\alpha}{|\nabla\alpha|}$.

Equation 6.7 shows that for a cell in computational domain, F_s is proportional to the average density in the cell. Clearly, the source term, F_s takes a non-zero value only in the cells through which the interface passes where $\nabla\alpha$ is not zero. The evolution of interface is tracked by solving Equation 6.4.

6.2.2 Numerical methods and simulation setup

The computational domain consists of a small cylindrical section $\Omega = [(x,y): 0\leq x\leq 60R, 0\leq y\leq 20R]$, where R refers to the radius of the droplet. The region equivalent to the size of the droplet, as observed in the experiment is marked in the computational domain and assigned a value of $\alpha = 1$, to represent the dispersed phase. Thus, the droplet is allowed to start from the rest. It should be noted that the main objective of this study is to analyze the change in droplet dynamics, so pinch off mechanism has not been studied numerically.

The transient simulation is carried out by using explicit scheme. The pressure velocity coupling is established through PISO (Pressure –implicit with splitting of operators) scheme. The spatial discretization used in momentum equation is second order upwind differencing scheme. The calculation of gradients is based on the Green-Gauss Cell Based method. PRESTO (Pressure Staggering Option) scheme is employed for pressure interpolation. The interface construction in cells containing both dispersed as well the continuous phase is achieved by using Geometric Reconstruction scheme which was explained briefly in Section 6.1.3.

The computational domain for 2D axisymmetric case has been shown by the shaded region in Figure 6.2. The mesh in the domain consists of triangular elements, which is constructed using ANSYS ICEM. More details on the simulation have been summarized in Table 6.1. For 3D simulations a cylindrical domain containing tetrahedral elements is built. Mesh dependency test was done, and mesh containing 285,988 triangular elements and 3,924,911 tetrahedral elements were used for performing 2D axisymmetric and 3d simulations respectively.

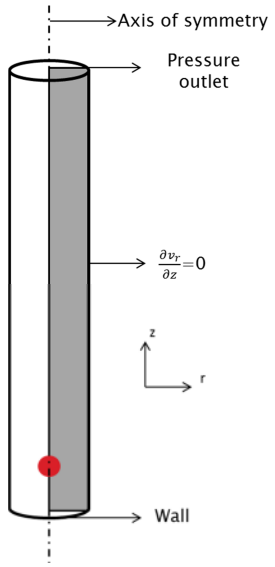

Figure 6.2 Computational domain for 2D axisymmetric simulation and boundary conditions.

Table 6.1 2D axisymmetric simulation specifications.

	Dispersed Phase	Continuous Phase
	Crude Oil	Water
Density	888.84 kg/m^3	999.5 kg/m^3
Viscosity	25.25 cP	1 cP
Simulation Parameters		
Domain Size	0.08 m X 0.25 m	
Number of cells	285,988	
Model	Volume of Fluid	

Chapter 7 Results and Discussion

The experiment and numerical methodology were described in the earlier chapters. In this chapter, the key observations and results from the experiment and the results from numerical simulations have been discussed.

7.1 Experimental Observations and Interpretation

7.1.1 Droplet size

In each of the runs during the experiment, the droplets were injected at a low flow rate, to suppress the contribution of inertial force. When the crude oil is injected in the tank, the droplet initially registers a gradual growth in size, at the tip of nozzle. Under static conditions, the pinch off mechanism of the droplet is governed by balance between buoyancy force, gravitational force and interfacial tension force. The droplet grows until it acquires enough buoyancy to overcome the interfacial tension, which tends to hold the droplet to the tip of the nozzle and ultimately pinches off [16]. Figure 7.1 illustrates the comparison between the droplet diameter found in experiment and one predicted from the correlation given by Equation 1.1. The deviation was found to be less than 6%.

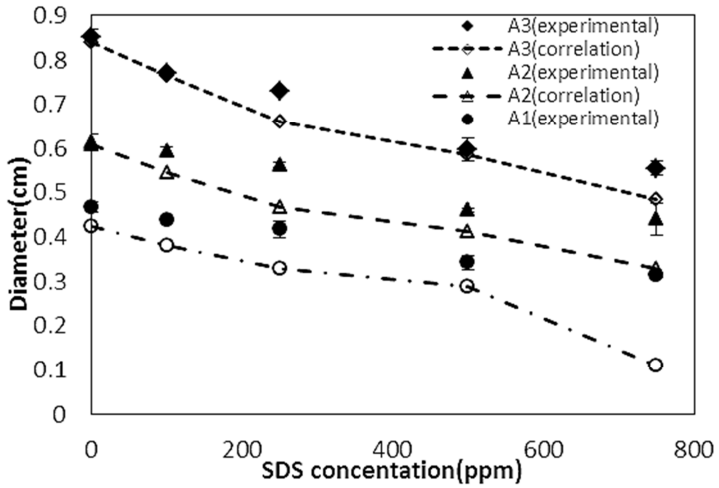

Figure 7.1 Dependence of droplet size on the surfactant concentration.

It was observed that as the surfactant concentration was increased, there was a decrease in size of the droplet produced at the nozzle. One possible explanation for this observation could be, with lowering interfacial

tension the interfacial tension force on the droplet decreases. So, the net buoyancy required for the droplet to pinch off falls and this results in formation of a smaller sized droplet.

7.1.2 Trajectory and shape of droplet

The trajectory adopted by the droplets, during their rise, is primarily dependent on their shape, which in turn is function of the *Re* and *Eo*. The smaller droplets (< 5mm) assumed the ellipsoidal shape and moved in rectilinear paths. These droplets were seen to exhibit axisymmetry even at higher concentrations of the surfactant. However, the larger droplets(>6mm) were initially found to assume ellipsoidal shape at the point of release but became more distorted as they rose in the water column, when fair amount of the surfactant was adsorbed on to its surface. These droplets exhibited oscillations about the horizontal plane and were found to travel in zigzag path.

Figures 7.2 and 7.3 show the trajectories assumed by the droplets emerging from nozzle A1, A2 and A3 respectively, in medium without surfactant and the one with 750 ppm. The snapshot reveals the position of droplet after every 0.03s. As evident from the figure, in absence of a surfactant, even the larger droplets follow a rectilinear path with insignificant oscillation. However, at high surfactant concentration, droplets with high Reynolds number droplets deviate significantly from the vertical axis and begin to oscillate. Table 7.1 summarizes the observed trajectories of droplets at different surfactant concentrations. The path taken by the droplets depends on the structure of wake at its trailing end. The various kinds of wake structures commonly encountered were introduced in Chapter 3. In general, a closed wake with little or no circulation allows the droplet to rise in a rectilinear fashion. The unsteady wake, with asymmetric nature causes the droplet to acquire a zigzag path.

The flow around a droplet differs from that of rigid sphere, as the internal circulations inside the droplet delays the flow separation and the subsequent wake formation in the surrounding fluid [7]. This is true for fluid with low K and when system is relatively clean. In present case, K is pretty high and with increase in surface contamination, onset of wake and hence the oscillations happens at a lesser Re[47]. This can be noticed in the Table 7.1; with increase in surfactant concentration, the droplet departs from rectilinear path at *Re* as low as 200.

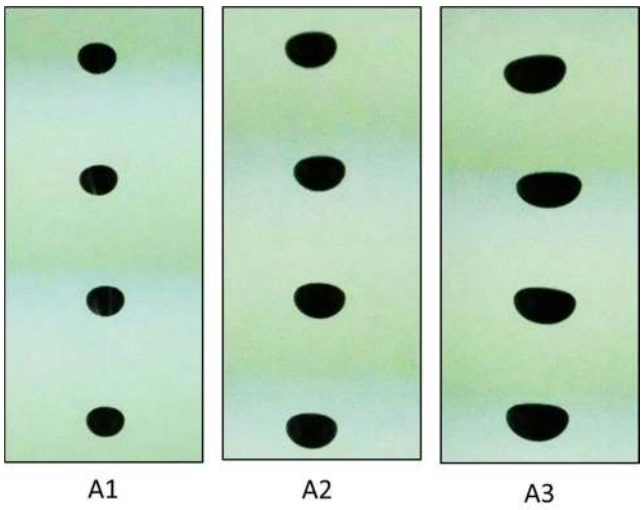

Figure 7.2 Trajectory of droplets in absence of surfactant.

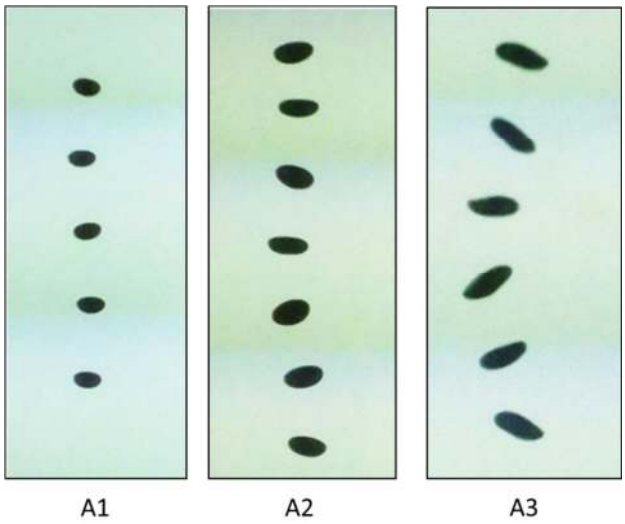

Figure 7.3 Trajectory of droplets at SDS concentration of 750 ppm.

Table 7.1 Trajectories of droplets depending on M and Re (Values in bracket indicate corresponding Re).

Nozzle/Surfactant concentration(ppm)	Morton Number(M)	A1	A2	A3
0	1.28×10^{-10}	Rectilinear(469)	Rectilinear(661)	Slightly zigzag(897)
100	1.30×10^{-9}	Rectilinear(416)	Rectilinear(610)	Oscillating-Zigzag(786)
250	2.34×10^{-9}	Rectilinear(363)	Rectilinear(538)	Oscillating-Zigzag(679)
500	5.87×10^{-9}	Rectilinear(264)	Oscillating-Zigzag(367)	Oscillating-Zigzag(458)
750	9.05×10^{-8}	Slightly zigzag(202)	Oscillating-Zigzag(296)	Oscillating-Zigzag(370)

The change in the trajectory of droplet ,i.e. from rectilinear to zigzag, at higher surfactant concentrations can be attributed to the oblateness imparted to the droplet and dampening of internal circulations which change the characteristics of wake, formed behind the droplet [48]. The onset of oscillation is due to the unsteady wakes which are asymmetric in nature.

7.1.3 Aspect Ratio

Drop deformation is governed by the competition between interfacial tension and viscous force due to flow. The images in Figure 7.4 are actual snapshots from the experiment, which illustrate the impact of surfactant on the shape of droplet, produced from nozzle A3.

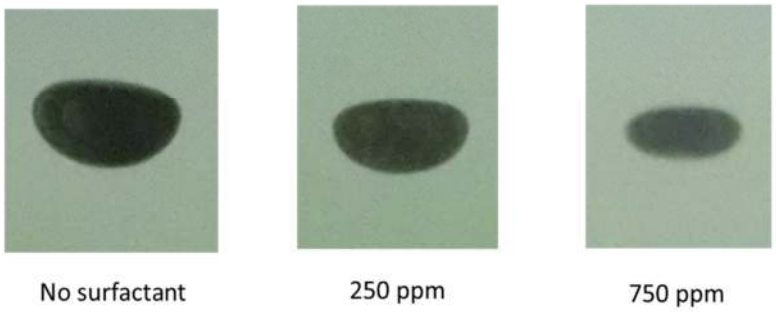

Figure 7.4 Effect of surfactant on the aspect ratio. Droplets are from nozzle A3.

In absence of a surfactant, the flattening of oil drops at the front end can be attributed to the increased hydrodynamic pressure, which can be associated to the stagnation point at the upper surface of the droplet. The lower surface of the oil droplet appears more spherical because of the more uniform distribution of the pressure (Figure 7.4). Pressure coefficients can often be employed to represent the pressure distribution around the droplet.

$$C_p = {}^{p\text{-}p_\infty}\Big/_{\frac{1}{2}\rho U^2} \qquad 7.1$$

Figure 7.5, from 3D simulations, shows the distribution of the pressure coefficient around the droplet. Clearly, pressure coefficients bear a higher value at the upper surface than on the lower part for droplet in environment with no surfactant. However, for flatter droplets (observed at higher surfactant concentrations), the

pressure coefficient distribution is more uniform. Other results from numerical simulation will be discussed later in this chapter.

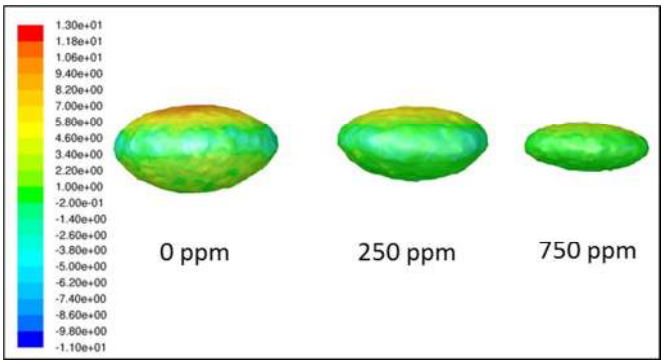

Figure 7.5 Pressure coefficients around droplet at various surfactant concentrations.

When a droplet rises in the medium with surfactant, surfactants are adsorbed on to the surface gradually. Due to this build up in surfactant concentration, the interfacial tension is lowered and the shear stresses imposed by the surrounding fluid causes the droplet to stretch by a greater extent, and the droplet elongates in transverse direction to acquire a flatter shape. This can be noticed in Figure 7.4. Thus, a reduction in the value of aspect ratio is observed. For the range of concentration of surfactant used in experiment, it was observed that the aspect ratio gradually decreased with increase in surfactant concentration in the continuous phase (Figure 7.6). Greater the surfactant concentration in bulk phase, greater will be the driving force for the transport of surfactant. This consequently increases the surface concentration of the surfactant and brings in drastic reduction in the interfacial tension.

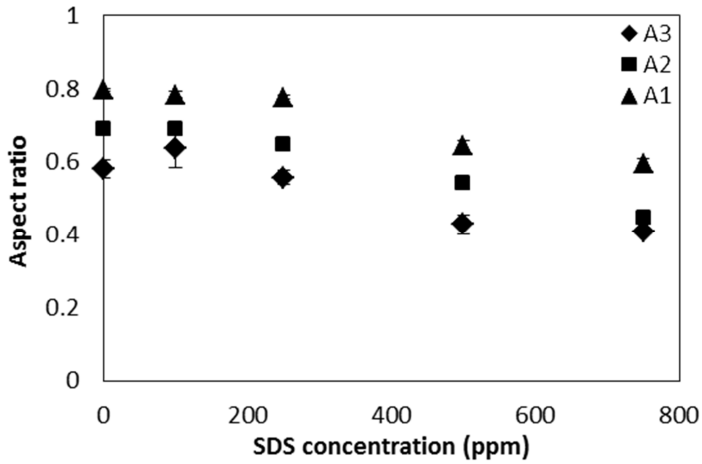

Figure 7.6 Effect of Surfactant concentrations on the aspect ratio.

Figure 7.7 shows the plot which compares the aspect ratio observed in the experiment with that estimated using the correlation (Equation 3.7, Page 14). The actual snapshots of the droplets, at various concentrations of surfactant are shown in Figure 7.8. A scan from bottom to top in each of the column indicates the reduction in aspect ratio of the droplet with the increase in surfactant concentration.

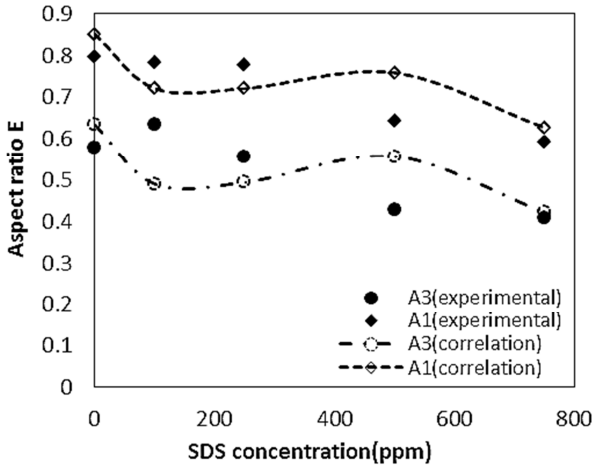

Figure 7.7 Comparison of droplet sizes found in experiment with correlation in Efremov et al[23].

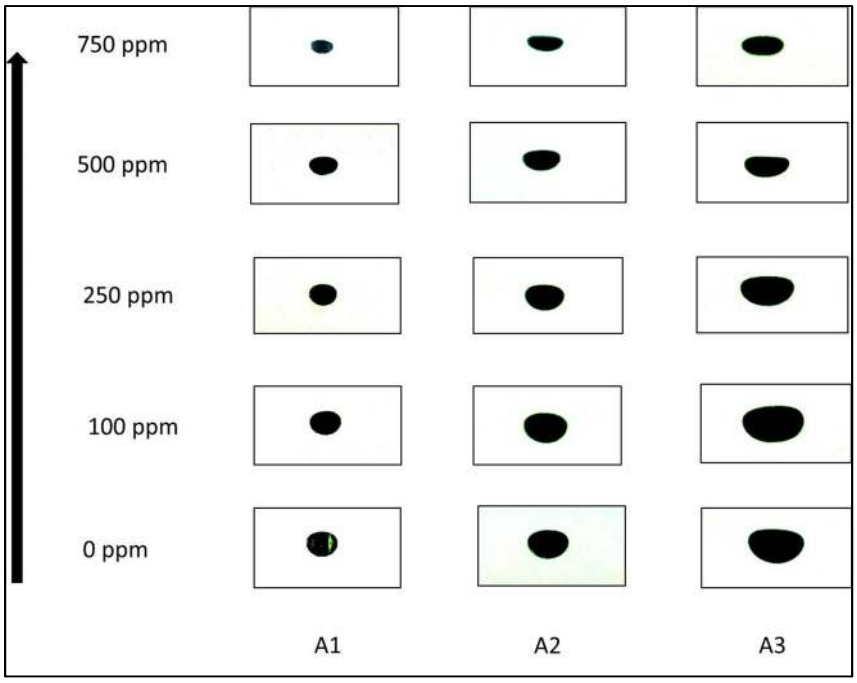

Figure 7.8 Snapshots of stable droplets from experiment at various surfactant concentrations.

7.1.4 Rise Velocity and drag coefficient

Whenever a droplet is released into stagnant medium, it initially accelerates. Eventually, a balance is established between the drag, buoyancy and gravitational forces and the droplet attains terminal velocity. For a droplet undergoing no mass loss, the volume can essentially be assumed to remain constant. Thus, the buoyancy and gravitational forces remain constant and thus, the rise velocity of the droplet solely depends on the magnitude of the drag force. The drag force, in turn depends on the shape of droplet and also on the influence of the surfactant on the motion of fluid inside the droplet. The dynamic rise velocity of droplets from A3 nozzle has been shown in Figure 7.9. It can be observed the rise velocity settles to a steady value in for droplet rising in medium containing no surfactant. On the other hand, the droplet moving in a high surfactant concentration environment acquires an oscillatory behavior and exhibits fluctuations in rise velocity initially before settling to a steady value.

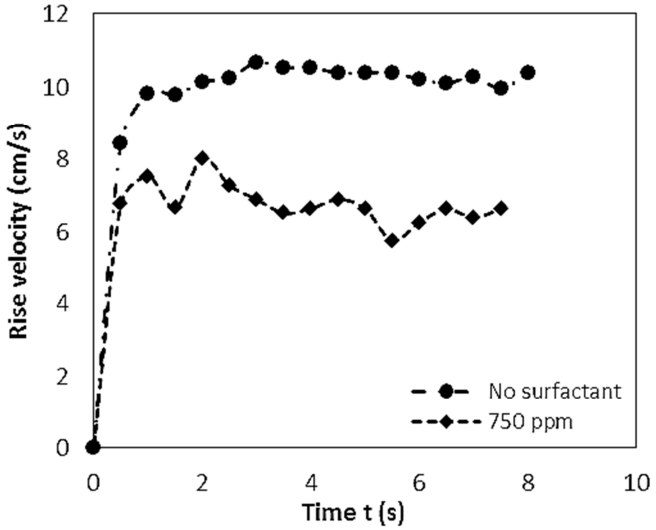

Figure 7.9 Dynamic rise velocities of droplets from nozzle A3.

The average rise velocity, which is the mean velocity with which droplet travels between 'A' and 'D' in Figure 5.2 (Page 33), for droplets from each of the nozzles has been shown in Figure 7.10. The average rise velocity decreases with increase in surfactant concentration. This drop in rise velocity can be attributed to the reduction in size of droplet as well as that in aspect ratio, with lowering of interfacial tension at the oil water interface. The flatter droplets witness an increase in drag force which contribute to their lower rise velocity[24]. The evaluation

of drag coefficient which is critical for calculation of drag force and hence the rise velocity has been described in the next section.

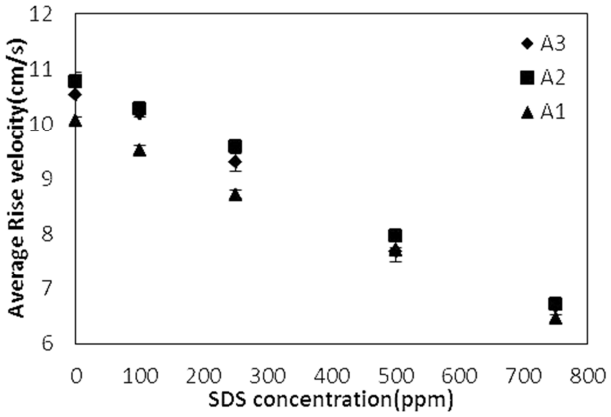

Figure 7.10 Average rise velocities for droplets observed in the experiment as a function of SDS concentration.

7.1.5 Drag coefficient evaluation

A short discussion on different correlations available in literature for evaluation of drag coefficient for fluid particles was done in Section 3.3.3. All of the correlations discussed are applicable for fluid spheres. But, in present investigation, droplets were found to deviate from spherical shape significantly. So, in present study a simple method has been proposed for evaluation of drag coefficient C_d. In order to evaluate C_d , a force balance was done around the droplet.

$$\frac{du}{dt} = \left(\frac{\rho_c - \rho_d}{\rho_d}\right) g - \frac{1}{2}\frac{C_d U^2 A_p \rho_c}{V_d} \qquad 7.2$$

The first term on right hand side of Equation 7.2 accounts for buoyancy and gravitational force and second term represents the drag force, acting on the droplet. The position of the droplet is obtained by integrating Equation 7.3.

$$u = {}^{dz}/_{dt} \qquad 7.3$$

The solution to above ODE's yields a height v/s time data. An initial guess values for C_d and A_p , which serve as parameters, was supplied for solving the ODE's. The obtained trajectory data was compared with that from the experiment. An objective function was constructed by evaluating the error between the height v/s time data, derived from the model and that from experiment.

$$Err = \sum_{i=0}^{N} \left(\frac{Z_{model} - Z_{experiment}}{Z_{experiment}} \right)^2 \quad 7.4$$

The objective function was then minimized to obtain the final value of C_d. The optimization was carried out in MATLAB®. In optimization scheme, C_d was used as an adjustable parameter to find the best fit of trajectory obtained by the model to one from experiment. The procedure has been summarized in Figure 7.11.

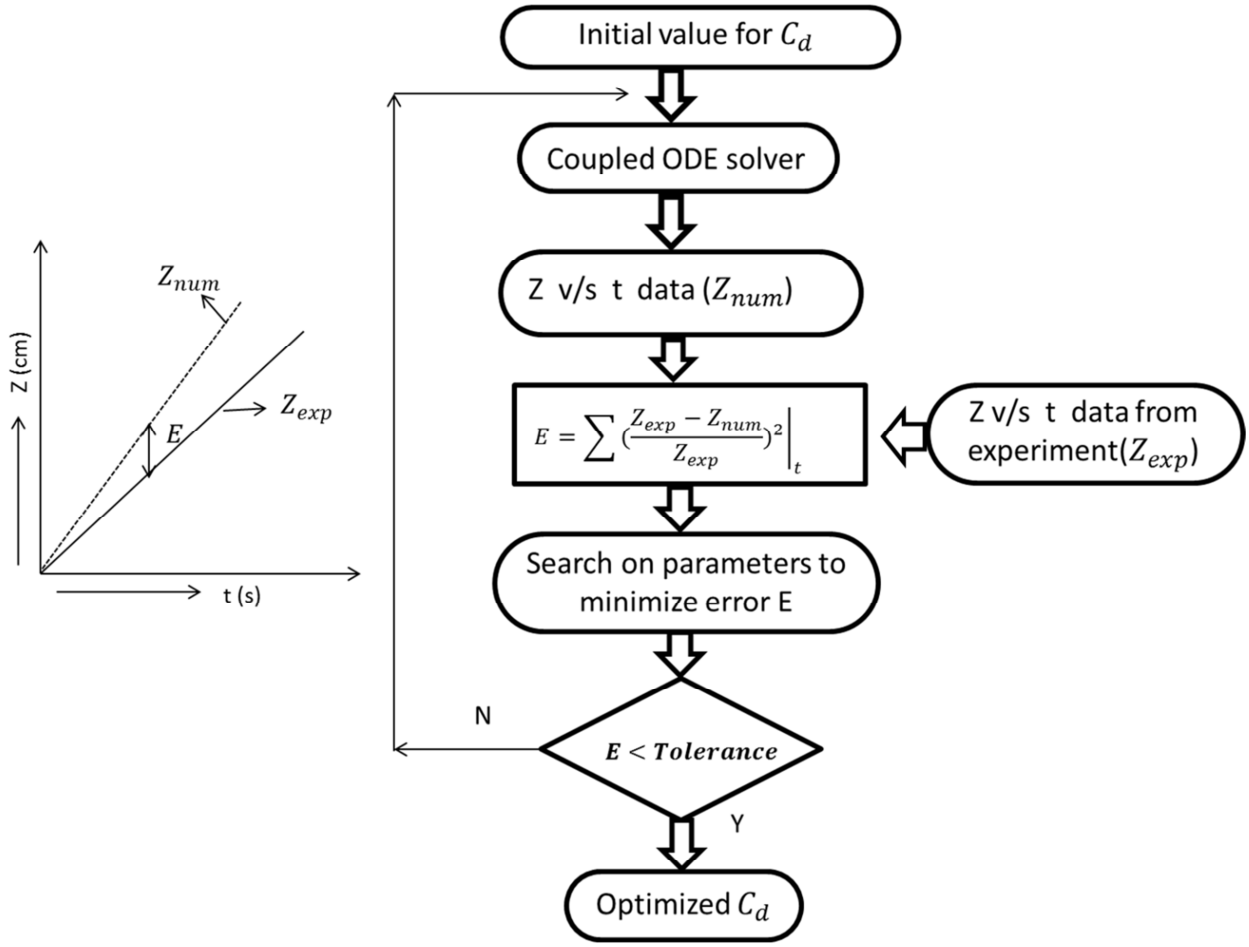

Figure 7.11 Steps undertaken for evaluation of drag coefficient.

The values of C_d for droplets thus obtained have been plotted in Figure 7.12 (for nozzle A3), against SDS concentration. The drag coefficients for equivalent rigid and fluid sphere (in pure medium) ,calculated from have also been plotted. Schiller Naumann drag correlation in widely used for rigid spheres for Re <800 given by Equation 7.5.

$$C_{d,rigid} = 1 + 0.15 Re^{0.687} \quad 7.5$$

The drag coefficient for fluid spheres was calculated using Equation 3.12. The effect of surfactant is depicted in Figure 7.12 (Cd_fluid _distorted represents the drag coefficients ellipsoidal droplets). The droplet in presence of surfactant become flatter and exhibits a higher drag coefficient and hence experiences higher drag force and rises with a lesser velocity.

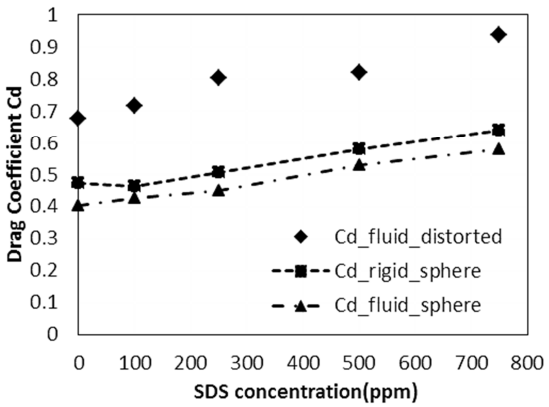

Figure 7.12. Drag coefficient for ellipsoidal droplets from the model compared with the drag coefficient obtained from correlations for equivalent rigid and fluid sphere.

The picture becomes clearer when Figure 7.13 is considered. It shows that, for a particular sized droplet, the drag coefficient increases with the increase in *M*, which can be attributed to increase in oblateness as well as change in characteristics of the internal circulation. The effect of surfactant on the drag coefficient is highest at the transition point, where motion changes from rectilinear to oscillatory[7, 20]. This can be seen in Figure 7.14, which shows that at transition point, (which is demarcated by a solid curve passing through all curves), the value of C_d witnesses an increase in its value. The drag contribution in region where droplet remains ellipsoidal and rises in rectilinear trajectory is mainly due to viscous drag. However, beyond transition point, where droplets exhibit oscillations, contribution of pressure drag and energy loss due to oscillations, contribute much more to the total drag and hence C_d increases [7].

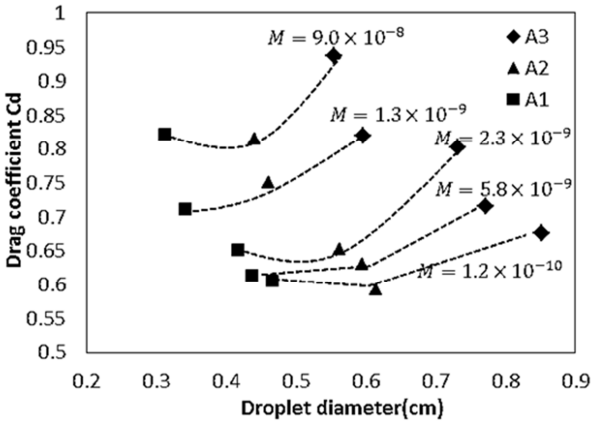

Figure 7.13 Drag coefficient of droplets from experiment as function of droplet diameters at various Morton numbers (M).

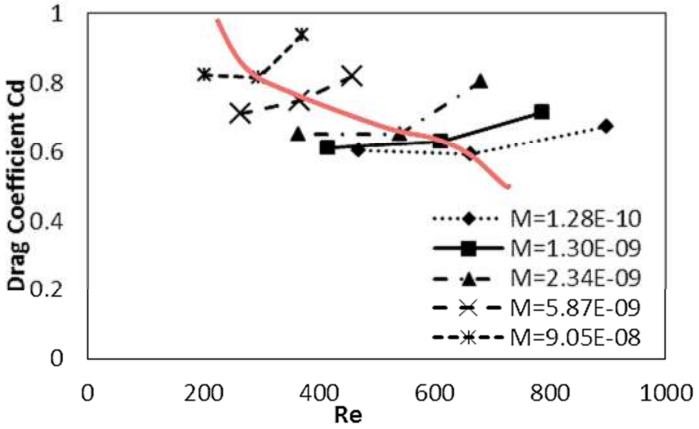

Figure 7.14 Drag coefficient variation as a function of Re at various Morton Numbers (M).

7.2 Numerical Results

Observations

One of the prime requirements of the numerical model developed is to simulate the deformations observed in the experiment. Figure 7.15 shows the contour plot for volume of fraction α, for droplets from A1 nozzle simulated with 2D axisymmetric assumption, and compares it with the snapshots of the stable oil droplets observed in the experiment. The qualitative result, depicting the shape of the droplet matches well with that in the experiment. It was mentioned in the earlier sections that the deformable interface of the droplet causes the development in the internal circulations. This fact is reaffirmed by the plot of velocity vectors (Figure 7.16) from simulations. The right portion of each image shows the associated vorticity contours. It can be seen that with

increase in surfactant concentration the droplet becomes flatter. The weakening of internal circulations and the oblateness imparted due to the presence of the surfactant reduces the angle of flow separation (measured from the front stagnation point).Consequently, the recirculating wake formed at the rear end of the droplet due to vorticity accumulation widens and reduces in length. The formation of an attached wake is enhanced by the tendency of surfactant to cut down the strength of internal circulations. For the simulated droplets, wake length for a droplet with no surfactant (Re= 470 was 0.011m whereas for 750 ppm case (Re= 200) it was about 0.008m.

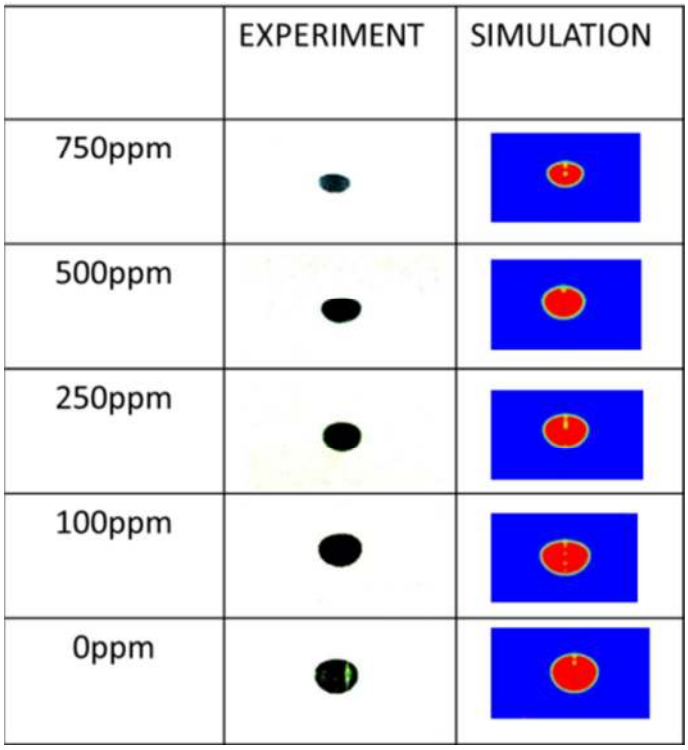

Figure 7.15 Comparison of simulated contour plots for axisymmetric droplets with actual snapshots from the experiment.

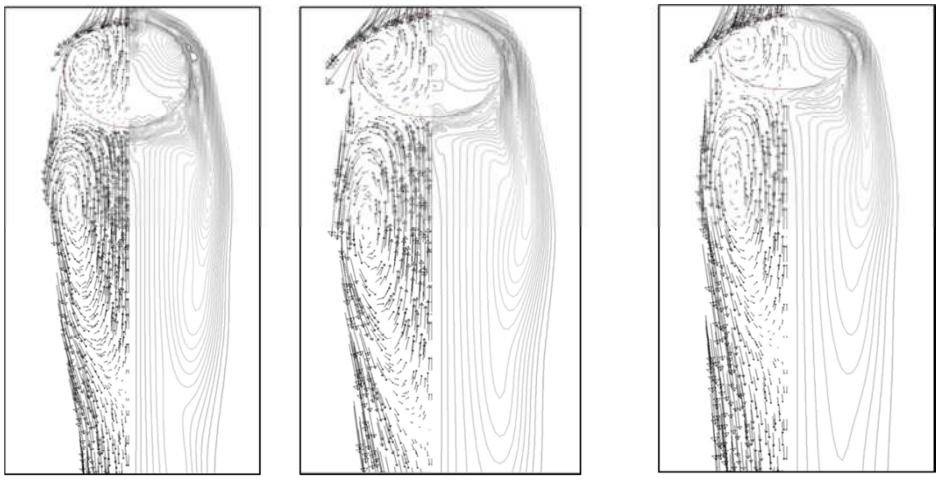

Figure 7.16 Velocity vectors and vorticity contours in simulated droplets at various surfactant concentrations.

Figure 7.17 shows the results from the simulation depicting the decreasing of aspect ratio with increase in surfactant concentration in the continuous phase. The simulation results reveal a trend similar to that observed during experiment and is in good agreement, with error of less than 8%. The comparison of average rise velocities of simulated axisymmetric droplets with changing SDS concentration with that from experiment has been shown in Figure 7.18. Again the agreement between the values predicted by the model with that of experiments seems to be satisfactory.

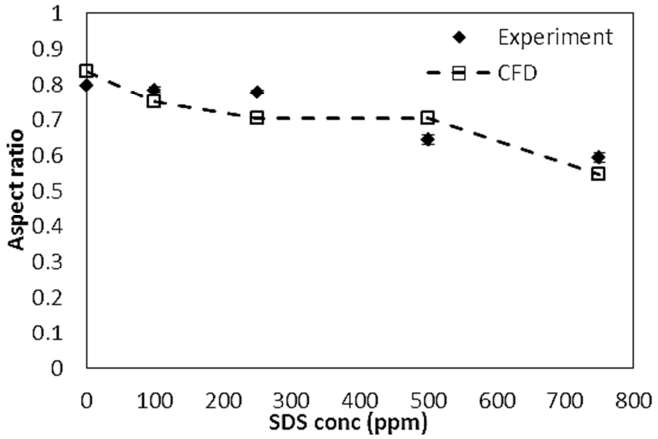

Figure 7.17 Aspect ratio of oil droplet as function of SDS concentration -simulation data compared with experimental data.

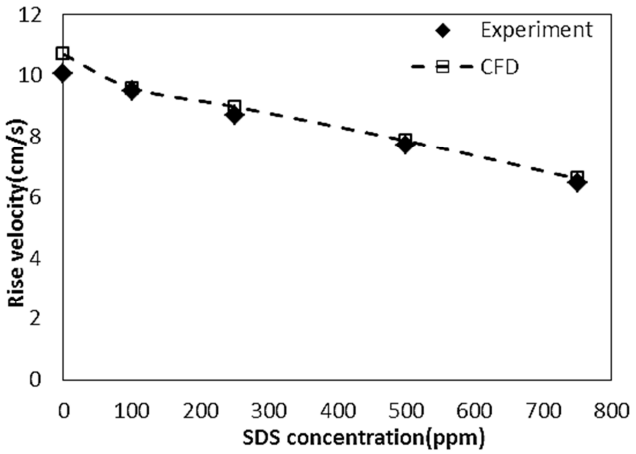

Figure 7.18 Average rise velocities of axisymmetric droplet as function of SDS concentration -simulation data compared with experimental data.

In addition to 2D axisymmetric simulations , complete 3D simulations were performed to mimic the behaviour of larger droplets from nozzle A3. In each of these simulations, region equal to the diameter of the droplet observed in experiment (at the time of pinch off) was initally marked with $\alpha = 1$,to represent the dispersed phase in the computational domain and released from rest. Figure 7.19 shows the comparison between the shape assumed by the droplets in simulation and experiment, at various surfactant concentrations.

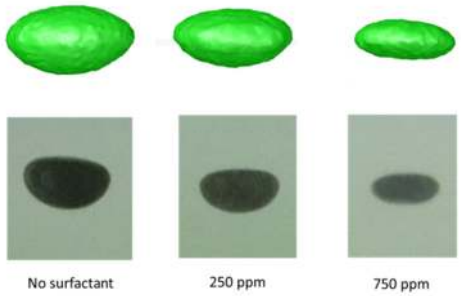

Figure 7.19 Qualitative result comparing the shapes predicted by 3d simulation with droplets from experiments at various surfactant concentrations.

Figures 7.20 and 7.21, reveal a good agreement between the values of aspect ratios and rise velocities predicted by the model with those observed in the experiment. The deviation in values was found to be within 10%.

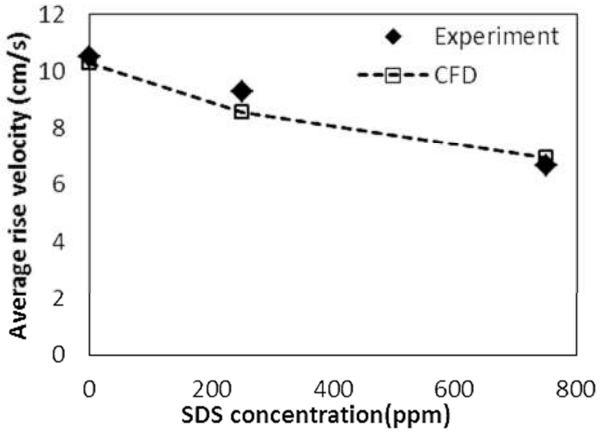

Figure 7.20 Average rise velocity variation with SDS concentration from 3d model and experiment for nozzle A3.

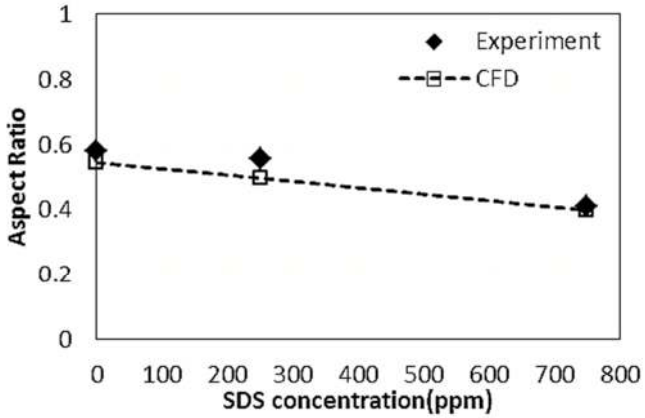

Figure 7.21 Aspect ratio variation with SDS concentration from 3d model and the experiment for nozzle A3.

Chang et al [37] in their work have concluded that for a droplet which is in motion , the convective flux for transport of surfactant is more significant than the diffusive flux so the equilibrium IFT should be attained more quickly than for static droplets.This was briefly explained in Chapter 5 follwed by calculation of adsorption time scales. In the models presented above ,the interfacial tension at oil-water interface was kept constant at the equilibrium values derived from the IFT measurements.

Chapter 8 Conclusions and Future work

An experimental and numerical investigation was carried out to analyze the effect of surfactant on the dynamics of crude oil droplet. Droplets ranging between 3 to 8mm were produced from three different nozzles and released into the quiescent water column, containing SDS surfactant. Pendant drop experiments were conducted in ambient cell for evaluating IFT at oil-water interface at different surfactant concentrations employing 'Axisymmetric drop shape analysis' (ADSA) method. It was observed that the increase in surfactant concentration resulted in,

- decrease in the size of droplet being generated at the tip of a particular nozzle;
- decrease in aspect ratio of the droplet, i.e. droplets assumed a more flatter shape and
- decrease in the rise velocities of the droplet.

The above results can be summarized by considering Figures 8.1 and 8.2. The former indicates the reduction in average rise velocity of droplet of a given size, with increase in surfactant concentration; which is basically due to the decrease in aspect ratio, shown by the latter plot.

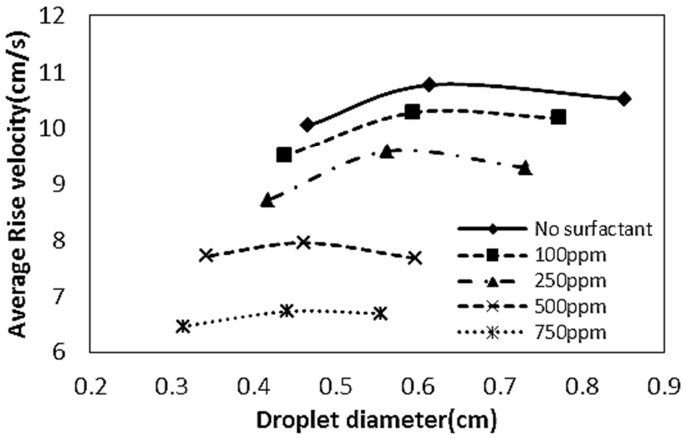

Figure 8.1 Average rise velocities as function of droplet diameter.

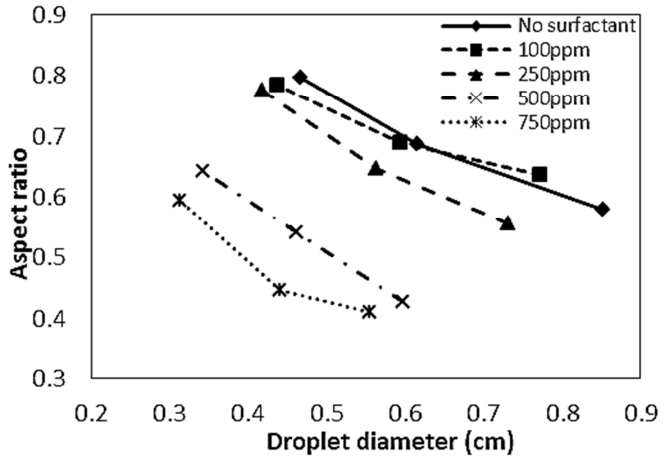

Figure 8.2 Aspect ratio as a function of droplet diameter at different SDS concentrations.

Drag coefficients were evaluated using simple force balance around the droplet and an increase in its value was observed at higher surfactant concentrations. A numerical model was developed to simulate the behavior of droplets observed in the experiment and the simulations were carried out in ANSYS Fluent®. To reduce the computational time, the droplets which were found to follow a rectilinear path were simulated using 2D axisymmetric assumption. Larger droplets which deviated significantly from the axis and underwent oscillations were simulated by a 3D model. The agreement between the results from experiments and simulations was found to be satisfactory.

In present study, experiments were conducted under ambient conditions, to analyze the effect of surfactant on the droplet dynamics. It has been established in previous studies that that adsorption characteristics of a surfactant is affected to some extent by presence of salt. Thus, in order to enhance the applicability of present study to an ocean environment, it would be important to study how the presence of salts affects the surfactant adsorption and hence influence the overall droplet dynamics.

In current numerical model the σ was assumed to be constant on the entire surface of droplet. However, the more accurate results can be obtained by inclusion of species transport equation in the model to account for the transportation of the surfactant from continuous phase to the interface and track the concentration of surfactant in the region near the interface in presence of the flow around the droplet. The lowering of interfacial tension in the cells through which the interface passes in the computational will depend on local concentration of the surfactant which can be obtained using Szyszkowski equation given by Equation 3.2.

Although the size of droplets observed in the experiment is far larger than that in an actual oil spill scenario, the present study does help in gaining a good understanding on how adsorption of surfactant can actually bring in change to physical parameters like rise velocity. Further, in the present study, the oil droplets were released in a quiescent medium. Turbulence is one aspect which is inseparable from the ocean environment. The presence of turbulence in addition to lowering of interfacial tension causes the larger droplets to disintegrate, and this offers another avenue which needs to be explored in detail.

References

[1] S.A. Socolofsky, E.E. Adams, Multi-phase plumes in uniform and stratified crossflow, Journal of Hydraulic Research, 40 (2002) 661-672.

[2] F. Chen, P. Yapa, Estimating the Oil Droplet Size Distributions in Deepwater Oil Spills, Journal of Hydraulic Engineering, 133 (2007) 197-207.

[3] B. Lehr, S. Bristol, A. Possolo, Oil Budget Calculator, Deep water Horizon, in, The Federal Interagency Solutions Group, Oil Budget Calculator Science and Engineering Team, 2010.

[4] E.B. Kujawinski, M.C. Kido Soule, D.L. Valentine, A.K. Boysen, K. Longnecker, M.C. Redmond, Fate of Dispersants Associated with the Deepwater Horizon Oil Spill, Environmental Science & Technology, 45 (2011) 1298-1306.

[5] F.H. Garner, P.J. Haycock, Circulation in Liquid Drops, Proceedings of the Royal Society of London. Series A. Mathematical and Physical Sciences, 252 (1959) 457-475.

[6] T. Wairegi, J.R. Grace, The behaviour of large drops in immiscible liquids, International Journal of Multiphase Flow, 3 (1976) 67-77.

[7] S. Winnikow, B.T. Chao, Droplet Motion in Purified Systems, Physics of Fluids, 9 (1966) 50-61.

[8] M. Wegener, A.R. Paschedag, Mass transfer enhancement at deformable droplets due to Marangoni convection, International Journal of Multiphase Flow, 37 (2011) 76-83.

[9] L.A. Bozzi, J.Q. Feng, T.C. Scott, A.J. Pearlstein, Steady axisymmetric motion of deformable drops falling or rising through a homoviscous fluid in a tube at intermediate Reynolds number, Journal of Fluid Mechanics, 336 (1997) 1-32.

[10] E.E. Adams , S.M. Masutani Experimental and Analytical Study of Multi-phase Plumes in a Stratified Ocean with Application to Deep Ocean Spills, in, 2002.

[11] S. Homma, J. Koga, S. Matsumoto, M. Song, G. Tryggvason, Breakup mode of an axisymmetric liquid jet injected into another immiscible liquid, Chemical Engineering Science, 61 (2006) 3986-3996.

[12] W.D. Harkins, F.E. Brown, The determination of surface tension (free surface energy), and the weight of falling drops, Journal of the American Chemical Society, 41 (1919) 499-524.

[13] Y.H. Mori, Harkins-brown correction factor for drop formation, AIChE Journal, 36 (1990) 1272-1274.

[14] R. Kumar, A unified approach to bubble and drop formation, Chemical Engineering Science, 26 (1971) 177-184.

[15] S. Ramakrishnan, R. Kumar, N.R. Kuloor, Studies in bubble formation—I bubble formation under constant flow conditions, Chemical Engineering Science, 24 (1969) 731-747.

[16] G.F. Scheele, B.J. Meister, Drop formation at low velocities in liquid-liquid systems: Part I. Prediction of drop volume, AIChE Journal, 14 (1968) 9-15.

[17] B.J. Meister, G.F. Scheele, Drop formation from cylindrical jets in immiscible liquid systems, AIChE Journal, 15 (1969) 700-706.

[18] M. Horvath, L. Steiner, S. Hartland, Prediction of drop diameter, hold-up and backmixing coefficients in liquid-liquid spray columns, The Canadian Journal of Chemical Engineering, 56 (1978) 9-18.

[19] J.A.C. Humphrey, R.L. Hummel, J.W. Smith, Note on the mass transfer enhancement due to circulation in growing drops, Chemical Engineering Science, 29 (1974) 1496-1500.

[20] R. Clift, J.R. Grace, M.E. Weber, Bubbles, Drops, and Particles, Dover Publications, 2005.

[21] E. Michaelides, Particles, Bubbles and Drops: Their Motion, Heat and Mass Transfer, World Scientific, 2006.

[22] R.M. Wellek, A.K. Agrawal, A.H.P. Skelland, Shape of liquid drops moving in liquid media, AIChE Journal, 12 (1966) 854-862.

[23] G.I. Efremov, I.A. Vakhrushev, A study of the hydrodynamics of a three-phase fluidized bed, Chem Technol Fuels Oils, 5 (1969) 541-545.

[24] A.E. Hamielec, A.I. Johnson, Viscous flow around fluid spheres at intermediate reynolds numbers, The Canadian Journal of Chemical Engineering, 40 (1962) 41-45.

[25] V.Y. Rivkind, G.M. Ryskin, Flow structure in motion of a spherical drop in a fluid medium at intermediate Reynolds numbers, Fluid Dyn, 11 (1976) 5-12.

[26] Z.-G. Feng, E.E. Michaelides, Drag Coefficients of Viscous Spheres at Intermediate and High Reynolds Numbers, Journal of Fluids Engineering, 123 (2001) 841-849.

[27] K. Tsuchiya, L.-S. Fan, Near-wake structure of a single gas bubble in a two-dimensional liquid-solid fluidized bed: Vortex shedding and wake size variation, Chemical Engineering Science, 43 (1988) 1167-1181.

[28] L.-H. Chen, Y.-L. Lee, Adsorption behavior of surfactants and mass transfer in single-drop extraction, AIChE Journal, 46 (2000) 160-168.

[29] F. Changpeng, D. Jaroslaw, L.W. Calvin, Interfacial Tension Measurement in Fluid?Fluid Systems, in: Encyclopedia of Surface and Colloid Science, Second Edition, Taylor & Francis, 2007, pp. 2966-2980.

[30] A. Couper, R. Newton, C. Nunn, A simple derivation of Vonnegut's equation for the determination of interfacial tension by the spinning drop technique, Colloid & Polymer Sci, 261 (1983) 371-372.

[31] A.J.C. Bashforth F An attempt to test the Theory of capillary action, Cambridge University Press, London, 1883.

[32] J.M. Andreas, E.A. Hauser, W.B. Tucker, BOUNDARY TENSION BY PENDANT DROPS1, The Journal of Physical Chemistry, 42 (1937) 1001-1019.

[33] C.E. Stauffer, The Measurement of Surface Tension by the Pendant Drop Technique, The Journal of Physical Chemistry, 69 (1965) 1933-1938.

[34] Y. Rotenberg, L. Boruvka, A.W. Neumann, Determination of surface tension and contact angle from the shapes of axisymmetric fluid interfaces, Journal of Colloid and Interface Science, 93 (1983) 169-183.

[35] J. Van Hunsel, P. Joos, Adsorption kinetics at the oil/water interface, Colloids and Surfaces, 24 (1987) 139-158.

[36] O.I.d. Río, A.W. Neumann, Axisymmetric Drop Shape Analysis: Computational Methods for the Measurement of Interfacial Properties from the Shape and Dimensions of Pendant and Sessile Drops, Journal of Colloid and Interface Science, 196 (1997) 136-147.

[37] C.H. Chang, N.H.L. Wang, E.I. Franses, Adsorption dynamics of single and binary surfactants at the air/water interface, Colloids and Surfaces, 62 (1992) 321-332.

[38] C.-H. Chang, E.I. Franses, Adsorption dynamics of surfactants at the air/water interface: a critical review of mathematical models, data, and mechanisms, Colloids and Surfaces A: Physicochemical and Engineering Aspects, 100 (1995) 1-45.

[39] F.H. Harlow, J.E. Welch, Numerical Calculation of Time-Dependent Viscous Incompressible Flow of Fluid with Free Surface, Physics of Fluids, 8 (1965) 2182-2189.

[40] C.S. Peskin, B.F. Printz, Improved Volume Conservation in the Computation of Flows with Immersed Elastic Boundaries, Journal of Computational Physics, 105 (1993) 33-46.

[41] S. Osher, J.A. Sethian, Fronts propagating with curvature-dependent speed: Algorithms based on Hamilton-Jacobi formulations, Journal of Computational Physics, 79 (1988) 12-49.

[42] C.W. Hirt, B.D. Nichols, Volume of fluid (VOF) method for the dynamics of free boundaries, Journal of Computational Physics, 39 (1981) 201-225.

[43] R. Scardovelli, S. Zaleski, Direct Numerical simulation of free- surface and interfacial flow, Annual Review of Fluid Mechanics, 31 (1999) 567-603.

[44] W.J. Rider, D.B. Kothe, Reconstructing Volume Tracking, Journal of Computational Physics, 141 (1998) 112-152.

[45] D.L. Youngs, Time-dependent multi-material flow with large fluid distortion, in Numerical methods for Fluid dynamics Academic Press , New York, 1982.

[46] J.U. Brackbill, D.B. Kothe, C. Zemach, A continuum method for modeling surface tension, Journal of Computational Physics, 100 (1992) 335-354.

[47] J. Berghmans, Stability of gas bubbles rising in inviscid fluids, Chemical Engineering Science, 28 (1973) 2005-2011.

[48] H.A. Stone, Dynamics of Drop Deformation and Breakup in Viscous Fluids, Annual Review of Fluid Mechanics, 26 (1994) 65-102.

Appendix Permissions

The figures adopted from the literature appearing in the document have been included after seeking appropriate permissions from the concerned agencies/authors.

1. Figure 2.1

ELSEVIER LICENSE TERMS AND CONDITIONS

Feb 11, 2014

This is a License Agreement between Abhijit Rao ("You") and Elsevier ("Elsevier") provided by Copyright Clearance Center ("CCC"). The license consists of your order details, the terms and conditions provided by Elsevier, and the payment terms and conditions.

All payments must be made in full to CCC. For payment instructions, please see information listed at the bottom of this form.

Supplier	Elsevier Limited The Boulevard,Langford Lane Kidlington,Oxford,OX5 1GB,UK
Registered Company Number	1982084
Customer name	Abhijit Rao
Customer address	Louisiana State University Baton Rouge, LA 70803
License number	3285560065994
License date	Dec 10, 2013
Licensed content publisher	Elsevier
Licensed content publication	Chemical Engineering Science
Licensed content title	Breakup mode of an axisymmetric liquid jet injected into another immiscible liquid
Licensed content author	Shunji Homma,Jiro Koga,Shiro Matsumoto,Museok Song,Grétar Tryggvason
Licensed content date	June 2006
Licensed content volume number	61
Licensed content issue number	12
Number of pages	11
Start Page	3986
End Page	3996
Type of Use	reuse in a thesis/dissertation
Intended publisher of new work	other
Portion	figures/tables/illustrations
Number of figures/tables/illustrations	1
Format	electronic
Are you the author of this Elsevier article?	No
Will you be translating?	No
Title of your thesis/dissertation	EFFECT OF SURFACTANT ON THE DYNAMICS OF A CRUDE OIL DROPLET RELEASED IN QUIESCENT WATER COLUMN

2. Fig 3.1, 3.2 and 3.4

Abhijit Rao <arao4@tigers.lsu.edu>

Permission for using figures from Bubbles, drops, and particles, 2005, by Roland Clift; John R Grace; Martin E Weber

3 messages

Abhijit Rao <arao4@tigers.lsu.edu> Tue, Feb 11, 2014 at 1:09 AM
To: r.clift@surrey.ac.uk, jgrace@chbe.ubc.ca

Dear Dr Clift, Dr Grace ,
I'm a graduate student in Department of Chemical Engineering at Louisiana State University. I would like to use Figures 2.5,7.3 and 7.13 in my Masters thesis from the book titled "Bubbles, Drops and Particles" authored by R. Clift , J.R Grace and M.E Weber - ISBN 978-0-486-44580-9. I would be grateful to you if I can be granted permission to use the above mentioned images in the document.

Thanks
–
Abhijit Rao
Graduate Student,
Cain Department of Chemical Engineering,
Louisiana State University

---

r.clift@surrey.ac.uk <r.clift@surrey.ac.uk> Tue, Feb 11, 2014 at 8:13 AM
To: arao4@tigers.lsu.edu
Cc: jgrace@chbe.ubc.ca

That's fine by me.

Roland Clift

Professor Roland Clift CBE FREng FIChemE HonFCIWEM FRSA
Emeritus Professor of Environmental Technology
Centre for Environmental Strategy (D3)
University of Surrey
Guildford
Surrey GU2 7XH

View the first Roland Clift Lecture on Industrial Ecology at:

http://www.surrey.ac.uk/ces/news/key_events/roland_clift/

From: Abhijit Rao [mailto:arao4@tigers.lsu.edu]
Sent: 11 February 2014 07:10

To: Clift R Prof (Centre Env. Strategy); jgrace@chbe.ubc.ca
Subject: Permission for using figures from Bubbles, drops, and particles, 2005, by Roland Clift; John R Grace; Martin E Weber

[Quoted text hidden]

John Grace <jgrace@chbe.ubc.ca> Tue, Feb 11, 2014 at 10:18 AM
To: Abhijit Rao <arao4@tigers.lsu.edu>

OK also with me. Thank you for asking asking and good luck. John Grace

3. Figure 4.5

Payment Information

Abhijit Rao
arao4@tigers.lsu.edu
+1 (225)5783052
Payment Method: n/a

Order Details

Encyclopedia of surface and colloid science

Order detail ID:	64200149
Order License Id:	3292100009044
ISBN:	978-0-8493-9615-1
Publication Type:	Book
Publisher:	TAYLOR & FRANCIS GROUP LLC
Author/Editor:	SOMASUNDARAN, PONISS

Permission Status: Granted

Permission type: Republish or display content
Type of use: Republish in a thesis/dissertation

Requestor type	Academic institution
Format	Electronic
Portion	chart/graph/table/figure
Number of charts/graphs/tables/figures	3
Title or numeric reference of the portion(s)	Figure 2, Figure 3, Figure 8
Title of the article or chapter the portion is from	MEASUREMENT OF INTERFACIAL TENSION IN FLUID-FLUID SYSTEMS
Editor of portion(s)	N/A
Author of portion(s)	N/A
Volume of serial or monograph	N/A
Page range of portion	3153-3158
Publication date of	12 Dec 2007

Rights for	Main product
Duration of use	Life of current edition
Creation of copies for the disabled	no
With minor editing privileges	no
For distribution to	United States
In the following language(s)	Original language of publication
With incidental promotional use	no
Lifetime unit quantity of new product	0 to 499
Made available in the following markets	education
The requesting person/organization	ABHIJIT RAO
Order reference number	
Author/Editor	ABHIJIT RAO
The standard identifier	Document
Title	EFFECT OF SURFACTANT ON THE DYNAMICS OF A DROPLET RELEASED IN THE QUIESCENT MEDIUM
Publisher	LSU
Expected publication date	May 2014
Estimated size (pages)	80

4. Figure 4.7

ELSEVIER LICENSE TERMS AND CONDITIONS

Feb 11, 2014

This is a License Agreement between Abhijit Rao ("You") and Elsevier ("Elsevier") provided by Copyright Clearance Center ("CCC"). The license consists of your order details, the terms and conditions provided by Elsevier, and the payment terms and conditions.

All payments must be made in full to CCC. For payment instructions, please see information listed at the bottom of this form.

Supplier	Elsevier Limited The Boulevard,Langford Lane Kidlington,Oxford,OX5 1GB,UK
Registered Company Number	1982084
Customer name	Abhijit Rao
Customer address	Louisiana State University Baton Rouge, LA 70803
License number	3285481155666
License date	Dec 10, 2013
Licensed content publisher	Elsevier
Licensed content publication	Journal of Colloid and Interface Science
Licensed content title	Determination of surface tension and contact angle from the shapes of axisymmetric fluid interfaces
Licensed content author	Y Rotenberg,L Boruvka,A.W Neumann
Licensed content date	May 1983
Licensed content volume number	93
Licensed content issue number	1
Number of pages	15
Start Page	169
End Page	183
Type of Use	reuse in a thesis/dissertation
Portion	figures/tables/illustrations
Number of figures/tables/illustrations	1
Format	electronic
Are you the author of this Elsevier article?	No
Will you be translating?	No
Title of your thesis/dissertation	EFFECT OF SURFACTANT ON THE DYNAMICS OF A CRUDE OIL DROPLET RELEASED IN QUIESCENT WATER COLUMN
Expected completion date	May 2014
Estimated size (number	80

5. Figure 4.8 and Figure 4.9

JOHN WILEY AND SONS LICENSE TERMS AND CONDITIONS

Dec 10, 2013

This is a License Agreement between Abhijit Rao ("You") and John Wiley and Sons ("John Wiley and Sons") provided by Copyright Clearance Center ("CCC"). The license consists of your order details, the terms and conditions provided by John Wiley and Sons, and the payment terms and conditions.

All payments must be made in full to CCC. For payment instructions, please see information listed at the bottom of this form.

License Number	3285480604399
License date	Dec 10, 2013
Licensed content publisher	John Wiley and Sons
Licensed content publication	AIChE Journal
Licensed content title	Adsorption behavior of surfactants and mass transfer in single-drop extraction
Licensed copyright line	Copyright © 2000 American Institute of Chemical Engineers (AIChE)
Licensed content author	Liang-Huei Chen,Yuh-Lang Lee
Licensed content date	Apr 16, 2004
Start page	160
End page	168
Type of use	Dissertation/Thesis
Requestor type	University/Academic
Format	Electronic
Portion	Figure/table
Number of figures/tables	2
Original Wiley figure/table number(s)	Figure 2 and Figure 3
Will you be translating?	No
Total	0.00 USD

6. Figure 4.10

ELSEVIER LICENSE
TERMS AND CONDITIONS

Dec 12, 2013

This is a License Agreement between Abhijit Rao ("You") and Elsevier ("Elsevier") provided by Copyright Clearance Center ("CCC"). The license consists of your order details, the terms and conditions provided by Elsevier, and the payment terms and conditions.

All payments must be made in full to CCC. For payment instructions, please see information listed at the bottom of this form.

Supplier	Elsevier Limited The Boulevard,Langford Lane Kidlington,Oxford,OX5 1GB,UK
Registered Company Number	1982084
Customer name	Abhijit Rao
Customer address	Louisiana State University Baton Rouge, LA 70803
License number	3286290662846
License date	Dec 12, 2013
Licensed content publisher	Elsevier
Licensed content publication	Colloids and Surfaces
Licensed content title	Adsorption kinetics at the oil/water interface
Licensed content author	J. Van Hunsel,P. Joos
Licensed content date	15 May 1987
Licensed content volume number	24
Licensed content issue number	2–3
Number of pages	20
Start Page	139
End Page	158
Type of Use	reuse in a thesis/dissertation
Intended publisher of new work	other
Portion	figures/tables/illustrations
Number of figures/tables/illustrations	1
Format	electronic
Are you the author of this	No

Elsevier article?	
Will you be translating?	No
Title of your thesis/dissertation	EFFECT OF SURFACTANT ON THE DYNAMICS OF A CRUDE OIL DROPLET RELEASED IN QUIESCENT WATER COLUMN
Expected completion date	May 2014
Estimated size (number of pages)	80
Customer Tax ID	726000848
Elsevier VAT number	GB 494 6272 12
Permissions price	0.00 USD
VAT/Local Sales Tax	0.00 USD / 0.00 GBP
Total	0.00 USD

Vita

Abhijit Rao, was born in January, 1986, in Tirthahalli, Karnataka, India. He completed his Bachelor's degree in Chemical Engineering at Visvesvaraya Technological University, Belgaum, India, in June 2007. He worked with Reliance Industries Ltd, India , from Aug 2007 to June 2010 , as a Process Engineer. After a brief stint in industry he joined Louisiana State University in Fall 2010 to pursue graduate studies in Cain Department of Chemical Engineering. He will be continuing with his Doctoral Program in Chemical Engineering at LSU. Abhijit expects to graduate with Master's degree in May 2014.